The insulin receptor adaptor IRS2 is an APC/C substrate that promotes cell cycle protein expression and a robust spindle assembly checkpoint

Sandhya Manohar[1], Qing Yu[1], Steven P. Gygi[1], Randall W. King[1,2*]

1. Department of Cell Biology, Harvard Medical School, Boston, Massachusetts 02115, USA.
2. Lead contact

* Correspondence: randy_king@hms.harvard.edu

Summary

Insulin receptor substrate 2 (IRS2) is an essential adaptor that mediates signaling downstream of the insulin receptor and other receptor tyrosine kinases. Transduction through IRS2-dependent pathways is important for coordinating metabolic homeostasis, and dysregulation of IRS2 causes systemic insulin signaling defects. Despite the importance of maintaining proper IRS2 abundance, little is known about what factors mediate its protein stability. We conducted an unbiased proteomic screen to uncover novel substrates of the Anaphase Promoting Complex/Cyclosome (APC/C), a ubiquitin ligase that controls the abundance of key cell cycle regulators. Surprisingly, we found that IRS2 levels are regulated by APC/C activity and that IRS2 is a direct APC/C target in G_1. Consistent with the APC/C's role in degrading cell cycle regulators, we find that IRS2-null cells are deficient in proteins involved in cell cycle progression and display spindle assembly checkpoint defects during M-phase. Together, these findings reveal a new pathway for IRS2 turnover and indicate that IRS2 is a critical component of the cell cycle control system in addition to acting as an essential metabolic regulator.

Keywords

Anaphase-Promoting Complex/Cyclosome; ubiquitin; cell cycle; insulin signaling pathway; G_1

Introduction

The insulin and insulin-like growth factor 1 receptors (IR/IGF1R) are receptor tyrosine kinases that control metabolism, differentiation, and growth. Upon ligand binding at the cell surface, the activated IR/IGF1R undergoes a conformational change that allows it to auto-phosphorylate tyrosine residues on its cytoplasmic subunits (Haeusler et al., 2017). This facilitates the recruitment and phosphorylation of insulin receptor substrate (IRS) proteins, which serve as scaffolds to initiate downstream signaling (Copps and White, 2012). Two major pathways that are stimulated by this cascade are the PI3K-AKT and Ras-Raf-MAPK pathways, which coordinate metabolic homeostasis and growth, among other functions (Haeusler et al., 2017).

The most physiologically important and ubiquitously expressed IRS proteins are IRS1 and IRS2. Though IRS1 and IRS2 share similar structural and functional features, they have complementary roles and expression patterns that depend on tissue type and physiological state (Haeusler et al., 2017). These differences are illustrated by divergent phenotypes in knockout mice: whereas IRS1 knockout mice exhibit insulin resistance that is compensated by increased pancreatic β cell mass, IRS2 knockout mice exhibit β cell failure and resultant diabetes (Lavin et al., 2016). Distinct roles for IRS1 and IRS2 can also be observed within the same tissue. For example, in skeletal muscle, IRS1 is required for glucose uptake and metabolism, whereas IRS2 is important for lipid uptake and metabolism (Bouzakri et al., 2006; Long et al., 2011). Furthermore, recent work has shown that the ratio of IRS1 to IRS2 is important for hepatic glucose metabolism (Besse-Patin et al., 2019). Thus, maintaining proper IRS1 and IRS2 levels is critical for systemic and cellular homeostasis.

The ubiquitin-mediated proteolysis of IRS proteins is important for restraining signaling through the IR/IGF1R. For example, both IRS proteins are targeted for proteasomal destruction following persistent insulin or IGF1 stimulation in a negative feedback loop that attenuates PI3K-AKT signaling (Copps and White, 2012; Scheufele et al., 2014). In mice, removal of a ubiquitin ligase that is responsible for IGF1-induced degradation of IRS1 enhances insulin sensitivity and increases plasma glucose clearance (Scheufele et al., 2014). Though several ubiquitin ligases have been reported to control IRS1's proteasome-dependent degradation (Nakao et al., 2009; Rui et al., 2002; Shi et

al., 2011; Xu et al., 2008; Yi et al., 2013), only SOCS1/3 have been implicated in driving IRS2 turnover (Rui et al., 2002). This is an intriguing disparity because hepatic IRS1 remains stable between fasting and feeding whereas IRS2 levels drop after feeding (Kubota et al., 2008), suggesting that IRS2 is less stable than IRS1 in some physiological contexts. Because SOCS1/3 also targets IRS1, there are no reports of ubiquitin ligases that target IRS2 but not IRS1, leaving a gap in our knowledge of how IRS1 and IRS2 are differentially regulated by the ubiquitin proteasome system.

The Anaphase-Promoting Complex/Cyclosome (APC/C) is a 1.2 mDa ubiquitin ligase that targets key cell cycle related proteins for destruction by the proteasome (Alfieri et al., 2017; Chang and Barford, 2014). To transfer ubiquitin to its substrates, the APC/C works with one of two co-activators: Cdc20 during M-phase or Cdh1 during G_1. These co-activators stimulate the catalytic activity of the APC/C and facilitate substrate recognition. APC/C^{Cdc20} and APC/C^{Cdh1} recognize substrates via short degron motifs in unstructured protein regions called destruction boxes (D-boxes) and KEN-boxes. An additional degron, called the ABBA motif, is used by APC/C^{Cdc20} only (Alfieri et al., 2017; Chang and Barford, 2014; Davey and Morgan, 2016).

To probe the substrate landscape of the APC/C, we conducted an unbiased proteomic screen by acutely blocking APC/C^{Cdh1} activity with small molecule APC/C inhibitors (apcin and proTAME) (Sackton et al., 2014; Zeng et al., 2010) in G_1 cells. Using this approach, we uncovered diverse putative APC/C^{Cdh1} substrates, including IRS2. We demonstrate that IRS2, but not IRS1, is a direct target of APC/C^{Cdh1}, thereby establishing a novel mode by which IRS1 and IRS2 are differentially regulated. Using IRS2 knockout cell lines, we show that IRS2 is important for the expression of proteins involved in cell cycle progression. We further show that genetic deletion of IRS2 perturbs spindle assembly checkpoint function. Taken together, these data establish a role for IRS2 in normal cell cycle progression, revealing new connections between an essential component of the growth factor signaling network and cell cycle regulation.

Results

Chemical proteomics reveals proteins whose abundances are APC/C^{Cdh1} regulated

To identify novel substrates and pathways regulated by APC/C^{Cdh1}, we designed an experiment that coupled small molecule inhibition of the APC/C in G_1 cells to high resolution tandem mass tag (TMT)-based quantitative proteomics (**Figure 1A**). Blocking Cdk4/6 activity inhibits Rb phosphorylation, causing cells to arrest at the G_1 restriction point (Ezhevsky et al., 1997). Thus, to generate a homogeneous population of G_1 cells, we treated asynchronous hTERT-RPE1 cells bearing fluorescent ubiquitination-based cell cycle indicator (FUCCI) constructs (Sakaue-Sawano et al., 2008) with the Cdk4/6 inhibitor palbociclib. Following G_1 arrest, cells were acutely treated with a combination of APC/C inhibitors (6 μM proTAME + 50 μM apcin) or vehicle (DMSO) for 8 hours. Cells were then collected for proteomic analysis with the expectation that APC/C-regulated proteins would be stabilized in cells treated with APC/C inhibitors compared to control cells (**Figure 1A**). The combined use of proTAME and apcin results in robust inhibition of the APC/C (Sackton et al., 2014), which guided our decision to use this treatment scheme. Moreover, this scheme was designed to specifically identify APC/C^{Cdh1} substrates rather than APC/C^{Cdc20} substrates since APC/C^{Cdh1} degrades Cdc20 during G_1 phase (Prinz et al., 1998). Illustrating this point, Cdc20 was undetectable in G_1 palbociclib-arrested cells (**Figure 1B**).

The experimental approach outlined in **Figure 1A** was validated using the FUCCI reporter system. This system relies on the expression of two stably integrated fluorescent fusion proteins—mAG1-geminin (1-110) and mCherry-Cdt1 (30-120)—to monitor the activity of endogenous cell cycle-related ubiquitin ligases APC/C^{Cdh1} and SCF^{Skp2}, respectively (Sakaue-Sawano et al., 2008). As expected, cells treated with palbociclib lost mAG1-geminin (1-110) protein expression over time due to APC/C^{Cdh1} activity while mCherry-Cdt1 (30-120) was stabilized, indicating G_1 arrest (**Figures S1A-S1B**). The addition of APC/C inhibitors in palbociclib-arrested cells rescued mAG1-geminin (1-110) levels (**Figures S1C-S1D**), confirming that this workflow stabilizes APC/C targets.

Using TMT-coupled quantitative proteomics, we identified and quantified relative abundances for ~8000 human proteins in G_1-arrested cells treated with or without APC/C inhibitors in biological triplicate (**Supplementary Table S1**). Notably, we detected 38 previously reported APC/C substrates in our dataset (**Figures 1C-1D; Supplementary Table S2).** Of these, 22 increased significantly ($p < 0.05$) under conditions of APC/C

inhibition. As an internal control, we detected a significant increase (p = 3.2 x 10^{-5}) in the abundance of peptides derived from the N-terminal 110 amino acids of geminin (GMNN). These residues are shared with the mAG1-geminin (1-110) reporter expressed in this cell line, confirming earlier fluorescence-based validation of our experimental system.

While the majority of the previously reported APC/C^{Cdh1} substrates that were quantified in our G_1 proteomic experiment were stabilized following APC/C inhibition, some remained constant. There are several possible explanations for this result. First, for proteins that were identified based on a small number of peptides, inadequate quantification may have resulted in inaccurate abundance assignments. Second, some substrates may be APC/C^{Cdh1}-accessible only under conditions or in tissue types that were not well modeled by the experimental parameters that we used. Third, some proteins (e.g. FBXW5, ZC3HC1) (Klitzing et al., 2011; Puklowski et al., 2011) were proposed to be APC/C^{Cdh1} substrates based on results obtained in Cdh1 overexpression systems, indicating that APC/C^{Cdh1} activity may be sufficient but not necessary to control their levels.

Of the 38 previously reported APC/C substrates that we identified, the median fold change under APC/C inhibition compared to DMSO was 1.147. Based on this, to identify new APC/C substrates, we screened for proteins that: (1) had a fold change ≥1.147 under APC/C inhibition, (2) were identified and quantified based on >1 peptide, and (3) had a p-value < 0.05 across the three biological replicates measured in this experiment. This narrowed our analysis to a subset of 204 proteins (**Supplementary Table S3**). Because the APC/C recognizes substrates based on D-box motifs (RxxL or the extended motif RxxLxxxxN) and KEN-box motifs (KEN), we used the SLiMSearch (Short Linear Motif Search) degron prediction tool(Davey and Morgan, 2016; Krystkowiak and Davey, 2017) to scan this 204-protein subset for proteins that contain these sequences. In order to classify a putative D- or KEN-box sequence as a probable physiological degron, we applied the following restrictions on the SLiMSearch (Krystkowiak and Davey, 2017) parameters: (1) similarity score ≥ 0.75; (2) consensus similarity is medium or high; (3) disorder score ≥ 0.4; (4) the putative degron must be intracellular and exist on a non-secreted protein. These cutoffs were determined based on those met by previously validated APC/C substrates (including those not identified in our dataset) and by the

physical restriction that APC/C activity occurs within the cell. Based on these thresholds, our analysis identified 26 proteins as potential D- and KEN-box containing APC/C^{Cdh1} substrates (**Table 1, Figure 1D**). Of these 26 proteins, 11 have previously been reported as direct APC/C substrates, validating internally that this analysis was useful for identifying APC/C substrates.

IRS2 levels are controlled by Cdh1 in a proteasome-dependent manner

Examining our 26-protein putative substrate list, we focused our attention on IRS2—one of two major adaptors that promotes signaling through the insulin and insulin-like growth factor 1 receptors (IR/IGF1R). Using conditions identical to those under which the proteomics experiment was conducted, we validated that IRS2 was upregulated at the protein level under APC/C inhibition in G_1-arrested RPE1 cells by immunoblot (**Figure 2A**). Seeking to further validate this result in a distinct physiological context, we asked whether APC/C inhibition in terminally differentiated C_2C_{12} myotubes also increases IRS2 protein abundance. C_2C_{12} myoblasts easily differentiate into multinucleated myotubes following serum withdrawal and supplementation with growth factors (**Figures S2A-S2B**). To validate that the APC/C is active in this system, we transfected C_2C_{12} myoblasts with a model APC/C substrate (N-terminal fragment of cyclin B1 fused to EGFP; NT-CycB-GFP), allowed cells to differentiate into myotubes, and found that APC/C inhibition stabilized NT-CycB-GFP (**Figure S2C**). Similarly, we found that acute APC/C inhibition in myotubes also resulted in an accumulation of IRS2 protein (**Figure 2B**), thereby validating this finding from our G_1 experiment in RPE1 cells in an independent system.

To exclude the possibility that the change in IRS2 abundance that we observed following APC/C inhibition was due to off-target effects of the small molecule APC/C inhibitors, we depleted Cdh1 using RNAi to block APC/C^{Cdh1} activity in RPE1, C_2C_{12}, and HeLa cells. In all three cell lines, we found that Cdh1 knockdown caused an accumulation of endogenous IRS2 compared to control-transfected cells (**Figure 2C-2E**).

We next sought to confirm that the increase in IRS2 protein observed under APC/C inhibition was due to impaired targeting of IRS2 to the proteasome. To test this, we arrested RPE1 cells in G_1 using palbociclib and acutely treated them with APC/C inhibitors and/or a proteasome inhibitor (MG132) for 8 hours. This experiment revealed that APC/C

inhibition or proteasome inhibition each resulted in an accumulation of IRS2 (**Figure 2F**). Notably, co-inhibition of the APC/C and the proteasome did not result in additional stabilization of IRS2, indicating that the increase in IRS2 we observed under APC/C inhibition was solely a consequence of its impaired ubiquitination and proteasomal degradation.

IRS2 levels and phosphorylation fluctuate in a cell-cycle dependent manner

To test whether IRS2 levels fluctuate during the cell cycle as expected for an APC/C substrate, we synchronized HeLa cells in early S-phase by double thymidine block and tracked IRS2 protein abundance leading into mitotic entry by immunoblot (**Figure 3A**). As is typical for known APC/C substrates, IRS2 levels correlated with cyclin B1 abundance and APC3 phosphorylation. To assess IRS2 levels at mitotic exit, we thymidine-nocodazole synchronized HeLa cells, released them into prometaphase, and tracked IRS2's abundance through mitotic exit (**Figure 3B**). Again, IRS2 protein abundance correlated with cyclin B1 levels and APC3 phosphorylation. The same behavior was observed in RPE1 cells that were synchronized in late G_2 by RO3306 treatment (Cdk1 inhibition) and tracked over the course of progression through M-phase and into G_1 (**Figure 3C**). Based on these data, we conclude that IRS2 protein levels fluctuate in a cell cycle dependent manner that is consistent with other known APC/C substrates.

In agreement with previous reports of mitotic phosphorylation of IRS2 by Plk1 (Chen et al., 2015), our cell cycle analysis experiments revealed that IRS2 displays a marked electrophoretic mobility shift consistent with mitotic phosphorylation. This may owe, at least in part, to Cdk1 activity given that HeLa cells released from a double thymidine block into Cdk1 inhibitor RO3306 did not display an observable shift in IRS2 mobility as compared to those released into control (DMSO) treatment (**Figure S3**). IRS2 abundance still peaked normally at this time point in the presence of RO3306, suggesting that the increase in IRS2 abundance was not dependent on Cdk1 activity. Together, these results support previous findings (Chen et al., 2015) that IRS2 is subject to cell-cycle dependent phosphorylation and that its abundance peaks in M-phase and falls in early G_1 in multiple cell lines.

Cdh1 control of IRS2 degradation depends on an IRS2 D-box motif

Based on its SLiMSearch prediction, IRS2 contains four minimal D-box motifs (RxxL), one extended D-box motif (RxxLxxxxN) and no KEN-box motifs. Of the four minimal D-box motifs, none bear strong consensus similarity to previously validated D-box motifs, and one exists in a highly structured region of the protein (Krystkowiak and Davey, 2017). Because of its high SLiMSearch parameter scores (**Table 1**), we focused our efforts on determining whether the extended D-box motif located in the C-terminal third of IRS2 is required for its APC/C^{Cdh1} dependent stability. IRS2's extended D-box (amino acids 972-980 in human IRS2) is highly conserved in placental mammals despite overall divergence in much of the C-terminus (**Figure 4A**), suggesting that this sequence likely has a conserved function.

To test whether IRS2's full D-box is relevant for its Cdh1-dependent degradation, we generated a mutant IRS2 construct bearing an R972A mutation (ΔD), which was expected to abrogate its function as a D-box (Glotzer et al., 1991). Using RPE1 cells stably expressing C-terminally HA-tagged IRS2-WT or IRS2-ΔD, we found that APC/C inhibition following G_1 arrest caused accumulation of IRS2-WT but not IRS2-ΔD (**Figure 4B**). The degree of accumulation of the WT protein depended on the dose of APC/C inhibitors used (**Figure S4A**). We were moreover able to repeat this result in terminally differentiated C_2C_{12} myotubes that stably expressed doxycycline-inducible, C-terminally HA-tagged IRS2-WT or IRS2-ΔD constructs that were treated with APC/C inhibitors (**Figure 4C**).

To further validate the Cdh1-dependence of IRS2's D-box motif, we asked whether Cdh1 knockdown by siRNA could stabilize the IRS2-ΔD protein. Using asynchronous RPE1 cells stably expressing C-terminally HA-tagged IRS2-WT and IRS2-ΔD, we found that Cdh1 knockdown by siRNA caused an accumulation of IRS2-WT relative to control-transfected cells but not IRS2-ΔD (**Figure 4D**). This result was repeated in HeLa cells stably expressing N-terminally FLAG-HA-tagged IRS2-WT and IRS2-ΔD constructs subject to the same conditions (**Figure 4E**).

The stable cell lines described above express tagged IRS2 variants at low levels comparable to the endogenous protein (**Figure S4B**), making it unlikely that the observed effects were protein overexpression artifacts. Notably, IRS1 (the other primary adaptor

protein for the IGF1R and IR) shares 75% sequence homology with IRS2's N-terminus and 35% homology with its C-terminus (Sun et al., 1995) but does not share the D-box motif found in IRS2's C-terminus (**Figure 4F**). In keeping with our hypothesis that Cdh1-mediated control of IRS2 is D-box dependent, IRS1 levels did not increase in G_1-arrested RPE1 cells treated with APC/C inhibitors as measured by either mass spectrometry (**Figure 4G**) or immunoblot (**Figure 4H**). Furthermore, while it did display a change in electrophoretic mobility compatible with mitotic phosphorylation, unlike IRS2, it did not decrease in abundance at mitotic exit in RPE1 cells (**Figure 4I**). Taken together, the findings described above indicate that APC/C^{Cdh1} controls IRS2 levels in manner that is dependent upon its C-terminal D-box motif.

IRS2 is required for normal expression of many proteins involved in mitosis

Many reported APC/C^{Cdh1} substrates (including several of those identified in our initial proteomics screen) are required for normal cell cycle progression. Because IR/IGF1R transduction promotes a variety of transcriptional programs (Copps and White, 2012), we hypothesized that IRS2 might promote the expression of proteins involved in cell cycle control. To investigate this, we generated two IRS2 knockout RPE1 cell lines using CRISPR/Cas9 (**Figure 5A)**, henceforth referred to as ΔIRS2-A and ΔIRS2-B. Using these cells, we again employed TMT-coupled quantitative proteomics. The proteomes of wild-type, ΔIRS2-A, and ΔIRS2-B cell lines were analyzed in biological triplicate, and relative abundances were ascertained based on TMT reporter ion signal-to-noise values. Hierarchical clustering indicated that the proteomes of the two knockout cell lines analyzed were more similar to each other than either knockout cell line was to wild-type (**Figure S5A**), indicating that deletion of IRS2 produced similar effects in both cell lines. In order to exclude aberrancies that may have accrued during the CRISPR process or as a result of clonal expansion, we focused the scope of our analysis to proteins that changed significantly ($p < 0.05$) by more than 20% in both IRS2 knockout clones relative to the WT cell line (**Figures 5B-5C**). We found 239 proteins that decreased by >20% in both IRS2 knockout lines relative to the wild type line and 300 proteins that increased by >20% (**Figures 5B-5C, S5B**).

We conducted gene enrichment analysis of the proteins that increased (**Figure S5C**) or decreased (**Figure 5D**) by >20% in both knockout cell lines relative to wild type cells. Of the 239 proteins that were depleted by >20% in both knockout cell lines, we found a statistical over-representation of proteins participating in metabolic processes characteristic of IR signal transduction. Notably, we also found an over-representation of proteins involved in mitotic cell cycle regulation in this subset (**Figure 5D**). This suite of proteins included regulators of mitotic entry and exit as well as several factors involved in spindle assembly (**Figure 5E**). Consistent with the fact that strong depletion of most critical cell cycle regulators renders cells inviable, most of the observed changes in cell cycle-related genes were relatively modest (**Figure S5D**). Based on these data, we conclude that IRS2 is important for promoting the expression of a suite of proteins involved in orchestrating the mitotic cell cycle, and deletion of IRS2 stunts their expression in RPE1 cells.

IRS2 expression promotes a functional spindle assembly checkpoint

Because many of the factors that were depleted in IRS2 knockout cell lines are known to be involved in regulating spindle assembly and mitotic exit, we asked whether IRS2 knockout cell lines display phenotypic differences from wild-type cells in terms of spindle assembly checkpoint function. Using a high content nuclear imaging assay to measure mitotic fraction based on DAPI staining intensity (Sackton et al., 2014), we asked whether IRS2 knockout cell lines display mitotic arrest differences compared to wild-type cells when treated with spindle poisons. Wild-type cells treated with nocodazole (a microtubule destabilizing agent) arrested in mitosis in a dose-dependent manner, whereas both IRS2 knockout cell lines displayed depressed mitotic arrest (**Figure 6A, Figure S6A**). This was also true to a lesser extent in the presence of S-trityl-L-cysteine (STLC), an Eg5 inhibitor (**Figure 6A**).

Using time lapse video microscopy, we found that untreated IRS2 knockout cell lines had no significant alteration in mitotic duration compared to wild-type cells (**Figure S6B**). In contrast, both IRS2 knockout cell lines had a significantly shorter mitotic duration compared to wild-type cells ($p < 0.0001$ in both cases) when treated with 300 nM nocodazole (**Figure 6B**). Importantly, wild-type cells expressing mAG1-geminin (1-101)—

an APC/C^{Cdc20} substrate that is stabilized by the spindle assembly checkpoint (Clijsters et al., 2013)— display an accumulation of mAG1 fluorescence early in mitotic arrest, consistent with checkpoint-mediated blockade of APC/C^{Cdc20}. In contrast, both IRS2 knockout cell lines display depressed mAG1 accumulation, consistent with higher APC/C^{Cdc20} activity due to a weakened checkpoint (**Figure 6C**). This phenotype, along with the shorter mitotic duration and lower mitotic fraction in the presence of spindle poisons, is consistent with cells bearing a defective mitotic spindle assembly checkpoint. Based on these data, we conclude that IRS2 promotes a functional spindle assembly checkpoint in RPE1 cells.

Discussion

Based on the results of an unbiased proteomic screen, we provide evidence that IRS2, a critical mediator of IR/IGF1R signaling, is a direct APC/C^{Cdh1} substrate. We demonstrate that IRS2 is stabilized by APC/C inhibition and Cdh1 knockdown in multiple cell types and that this depends on IRS2's C-terminal D-box motif. In contrast, we find that IRS1, a closely related IRS2 paralog that lacks a D-box, is not subject to regulation by the APC/C. Taken together, these results show that APC/C activity directly controls IRS2 levels in a D-box dependent manner.

We identified a high-mobility form of IRS2 that accumulates under APC/C inhibition, likely corresponding to a difference in phosphorylation given that IRS2 has ~150 annotated threonine, serine, and tyrosine phosphorylation sites (Hornbeck et al., 2015). This suggests that IRS2's APC/C-dependent stability could be regulated by phosphorylation, possibly at sites near or within the D-box, which is an intriguing topic for future study. Consistent with this, IRS2 phosphorylation is known to impact its stability in other contexts, including following prolonged exposure to insulin or following mTOR activation (Copps and White, 2012). Furthermore, there is a strong precedent for phospho-regulation of APC/C degrons modulating substrate stability under specific conditions (Holt, 2012; Mailand and Diffley, 2005; Wang et al., 2001).

Many APC/C substrates are involved in cell cycle regulation, and previous studies have suggested a relationship between IRS2 and cell cycle progression. IRS2 can stimulate cell cycle entry via Cdk4 activation (Chirivella et al., 2017) and is important for

sustaining proliferation in 32D myeloid cells and pancreatic β cells (Folli et al., 2011; Wu et al., 2009). Based on these findings and our identification of IRS2 as an APC/C substrate, we further investigated the role of IRS2 in regulating cell division. Proteomic analyses of RPE1 cells lacking IRS2 reveal lower expression of well-characterized cell cycle proteins compared to wild-type cells. Because these proteins are involved in critical processes like cytokinesis, DNA replication, cell cycle transitions, and spindle assembly, we investigated whether IRS2 knockout cell lines display cell cycle progression defects. We find that cells lacking IRS2 have an impaired ability to arrest following spindle assembly checkpoint activation in M-phase, thereby implicating IRS2 in promoting a functional spindle assembly checkpoint.

Despite the well-established importance of sustained IRS2 levels in many tissue types, little is known about what factors regulate its turnover. While several distinct ubiquitin ligases control IRS1 stability (Fbxw8, Cbl-b, Fbxo40, SOCS1/3, MG53, and others) (Nakao et al., 2009; Rui et al., 2002; Shi et al., 2011; Xu et al., 2008; Yi et al., 2013), only SOCS1/3 have been implicated in the ubiquitin mediated proteolysis of IRS2 (Rui et al., 2002) until now. Thus, our work establishes APC/C^{Cdh1} as the first known ubiquitin ligase that targets IRS2 but not IRS1. Furthermore, our results suggest that APC/C^{Cdh1}-mediated IRS2 degradation is relevant in broad biological contexts since we were able to demonstrate this mechanism of regulation in multiple cell lines.

Over the past several years, a number of connections between growth factor signaling and APC/C-mediated regulation have emerged. SKIL/SnoN, an APC/C substrate involved in TGFβ signaling, implicates APC/C activity in modulating the expression of TGFβ target genes (Wan et al., 2001). Another APC/C substrate, CUEDC2, controls the stability of the progesterone receptor (Zhang et al., 2007). Regarding IR/IGF1R signaling, connections to APC/C-mediated regulation have been more opaque. Multiple reports have shown that Cdh1 interacts with PTEN, a phosphatase that antagonizes signal transduction through the IR pathway by dephosphorylating phosphoinositide-3,4,5-triphosphate (PIP_3) (Choi et al., 2014; Song et al., 2011). Others have demonstrated that components of the mitotic checkpoint complex (which inhibit APC/C^{Cdc20}) potentiates IR signaling via IR endocytosis (Choi et al., 2019; Choi et al.,

2016). Despite these links, there have been no reports of direct APC/C substrates that are involved in IR signaling until now.

Based on the data presented here, we propose a model (**Figure 7**) in which IRS2's APC/C-mediated degradation in G_1 serves to limit IRS2-dependent signaling during G_1. Upon APC/C inactivation at the G_1/S boundary, IRS2 is able to accumulate and stimulate signaling required for normal progression through the latter stages of the cell cycle, including the expression of proteins required for mitotic spindle checkpoint function. This model is consistent with previous studies that implicate IRS2 in promoting the expression of cell cycle-related genes, including mitotic cyclins (A and B) in mouse granulosa cells (Lei et al., 2018). Furthermore, IR signal transduction promotes the expression of Plk1 (a mitotic kinase) and CENP-A (a centromere protein) in β cells through a mechanism that appears to depend on IRS2 rather than IRS1 (Folli et al., 2011; Shirakawa et al., 2017).

Our findings suggest that APC/C^{Cdh1} modulates IRS2-dependent signaling but not IRS1-dependent pathways. In IRS2-deficient mice with consequent type 2 diabetes, some have attributed the reduced β cell mass to a failure of β cells to re-enter the cell cycle following division (Folli et al., 2011). Our findings that APC/C^{Cdh1} inhibition stabilizes IRS2 and that IRS2 promotes the expression of cell cycle regulatory proteins, coupled with data from others showing that IRS2 can stimulate cell cycle entry (Chirivella et al., 2017), suggest that APC/C^{Cdh1} inhibition may represent a possible approach for stimulating proliferation in quiescent β cells via the stabilization of IRS2.

Acknowledgements

We thank the ICCB-Longwood Screening Facility at Harvard Medical School for assistance with high content imaging assays and the Nikon Imaging Facility at Harvard Medical School for assistance with time lapse and fluorescence microscopy. We thank Kyle Copps, Pere Puigserver, and Christine Vogel for feedback on the manuscript. This work was funded by NIH grant 1R35GM127032 to R.W.K.

Author Contributions

S.M. designed, performed, and analyzed all experiments aimed at identifying new APC/C substrates in RPE1 cells. S.M. performed all experiments characterizing IRS2 as an

APC/C substrate. S.M. generated all recombinant cell lines used in this study and the IRS2 CRISPR knockout cell lines. S.M. characterized mitotic arrest defects in IRS2 CRISPR knockout cell lines using time lapse microscopy and high-content imaging assays. S.M. prepared all samples for mass spectrometry with assistance from Q.Y.

Q.Y. and S.P.G. performed mass spectrometry analysis of G_1 RPE1 cells treated with APC/C inhibitors and IRS2 CRISPR knockout cell lines. Q.Y. and S.P.G. provided reagents.

R.W.K. assisted with experimental design and data analysis.

S.M. and R.W.K. conceived of the project and wrote the manuscript with input from both other authors.

Declaration of Interests

The authors declare no competing financial interests.

Main Figure Legends

Figure 1: *High resolution chemical proteomics reveals proteins whose abundances are APC/C regulated.*

(A) Workflow for the chemical proteomics experiment described in this study. Asynchronous RPE1 cells were arrested in 1 μM palbociclib (a Cdk4/6 inhibitor) for 20 hours, at which point they were acutely treated with either DMSO or a combination of 6 μM proTAME + 50 μM apcin (referred to as "APC/C inhibitors" or APCi). Cells were then collected at time 0 (t_0, the time of drug addition) or 8 hours after drug addition and were harvested for TMT-based proteomic identification and quantification. Samples were analyzed in biological triplicate within a 10-plex TMT label set, with the 10^{th} channel used as a bridge.

(B) Asynchronous RPE1 cells were treated with either DMSO or 1 μM palbociclib for 20 hours. Cells were harvested, and lysates were analyzed by immunoblot for the indicated proteins.

(C) Previously reported APC/C substrates that were identified in this study are plotted with their observed fold change in the APC/C inhibitor treated sample (APCi) relative to the DMSO treated sample. Error bars represent the standard deviation (SD) between the three biological replicates measured by MS. Asterisks indicate an abundance increase over control that is statistically significant (* : $p < 0.05$; ** : $p < 0.01$; *** : $p < 0.001$; **** : $p < 0.0001$)

(D) Volcano plot highlighting all published APC/C substrates identified in this study (blue) as well as proteins that (1) contain a high probability D- and/or KEN-box (D-box = green, KEN-box = pink, D- and KEN-boxes = purple), (2) increase ≥1.147-fold under APC inhibition, (3) were identified by >1 peptide, and (4) have a p-value < 0.05.

Figure 2: *IRS2 levels are controlled by Cdh1 in a proteasome-dependent manner*

(A) Cells were treated identically to what is described in **Figure 1A**, and IRS2 abundance was measured by immunoblot.

(B) C_2C_{12} myoblasts (Day 0) were induced to differentiate through serum withdrawal and supplementation with insulin, transferrin, and selenium (ITS). After three days of differentiation, myotubes were acutely treated with either DMSO or APC/C inhibitors (of 6 μM proTAME + 50 μM apcin). After eight hours of drug treatment, myotubes were collected and IRS2 levels from all samples were analyzed by immunoblotting.

(C)–(E) Asynchronous RPE1 (*C*), C_2C_{12} (*D*), and HeLa (*E*) cells were transfected with either a control or Cdh1-directed siRNA for 24 hours. siRNAs were washed out of cell culture media, and cells were allowed to grow for an additional 24 hours prior to collection and analysis of IRS2 and Cdh1 levels in lysate by immunoblot.

(F) RPE1 cells were arrested in G_1 with 1 μM palbociclib for 20 hours. Following G_1 arrest, cells were treated with DMSO, APC/C inhibitors (6 μM proTAME + 50 μM apcin), MG132 (10 μM), or a combination of APC/C inhibitors and MG132 for an additional 8 hours. Cells were harvested, and lysates were analyzed by immunoblot for IRS2 abundance.

Figure 3: *IRS2 levels and phosphorylation fluctuate in a cell-cycle dependent manner*

(A) HeLa cells were synchronized by double thymidine block and released into S-phase. Time points were taken every two hours for 14 hours. Lysates were harvested and analyzed by immunoblotting for IRS2 and cell cycle markers (APC3 phosphorylation and cyclin B1).

(B) HeLa cells were synchronized by thymidine-nocodazole block and released into prometaphase. Mitotic cells were collected by mitotic shake-off and re-plated. Time points were taken every two hours as cells exited M-phase. Lysates were harvested and analyzed by immunoblotting for IRS2 and cell cycle markers (APC3 phosphorylation and cyclin B1).

(C) RPE1 cells were synchronized in prometaphase by 7.5 μM RO3306 treatment. After 18 hours, cells were switched to fresh media and were allowed to enter mitosis (~35 minutes following drug removal). At mitotic entry, cells were collected by mitotic shake-off and were re-plated (0 hr). Time points were taken as cells exited M-phase and entered G_1. Lysates were harvested and analyzed by immunoblotting for IRS2 and cell cycle markers (APC3 phosphorylation and cyclin B1).

Figure 4: *Cdh1's ability to control IRS2 levels depends on a C-terminal D-box motif*

(A) (*top*) Schematic depicting IRS2's protein domain structure. PH = pleckstrin homology domain, PTB = phosphotyrosine binding domain, KRLB = kinase regulatory-loop binding region. IRS2's C-terminal full D-box motif is highlighted in red. (*bottom*) Comparison of IRS2's D-box conservation among placental mammals.

(B) RPE1 cells stably expressing lentivirus-derived, doxycycline-inducible, C-terminally HA-tagged IRS2 constructs were arrested in G_1 with 1 μM palbociclib for 20 hours. Following arrest, samples were either collected or DMSO or APC inhibitors (6 μM proTAME + 50 μM apcin) were added for an additional 8 hours. Quantification of immunoblots shown at right: HA levels were normalized to a loading control and are plotted relative to DMSO levels. Error bars = mean ± SEM. * : p=0.0187; ns : p=0.816

(C) C_2C_{12} myoblasts stably expressing lentivirus-derived, doxycycline-inducible, C-terminally HA-tagged IRS2 constructs were grown to confluence and switched to low serum media supplemented with ITS (differentiation media, DM) and doxycycline. Cells were allowed to differentiate into myotubes for three days (with media

refreshment every 24 hours), at which point (0 hr) either DMSO or APC/C inhibitors (6 μM proTAME + 50 μM apcin) for an additional 8 hours in the presence of doxycycline. Quantification of immunoblots shown at right: HA levels were normalized to a loading control and are plotted relative to DMSO levels. Error bars = mean ± SEM. * : p=0.0118; ns : p=0.910.

(D) Asynchronous RPE1 cells stably expressing lentivirus-derived, doxycycline-inducible C-terminally HA-tagged IRS2 constructs were transfected with a non-targeting (control) siRNA or an siRNA directed against Cdh1 for 24 hours. Quantification of immunoblots shown at right: HA levels were normalized to a loading control and are plotted relative to DMSO levels. Error bars = mean ± SEM. * : p=0.0132; ns : p=0.963.

(E) Asynchronous HeLa cells stably expressing lentivirus-derived, N-terminally FLAG-HA tagged IRS2 constructs were transfected with a non-targeting (control) siRNA or an siRNA directed against Cdh1 for 24 hours. Quantification of immunoblots shown at right: HA levels were normalized to a loading control and are plotted relative to DMSO levels. Error bars = mean ± SEM. * : p=0.0131; ns : p=0.803.

(F) Comparison of the Hs IRS2 D-box sequence with the aligned area on Hs IRS1.

(G) MS-quantified IRS1 and IRS2 abundance in G_1 APC inhibitor proteomics. IRS1 abundance was quantified based on 5 peptides (4 unique) in 3 biological replicates; IRS2 was quantified based on 3 peptides (all unique) in 3 biological replicates.

(H) RPE1 cells were subject to the same conditions described in Figure 1A, and cell lysates were analyzed by immunoblotting for IRS1 abundance

(I) RPE1 cells were synchronized in late G_2 with 7.5 μM RO3306 for 18 hours. Cells were released into fresh media and allowed to enter mitosis (~35 min post-drug removal) and were collected by mitotic shake-off. Mitotic cells were re-plated and collected at the indicated time points. Cell lysates were analyzed by immunoblotting for IRS1 abundance.

Figure 5: *IRS2 knockout cell lines are defective in mitotic cell cycle-related protein expression*.

(A) WT, ΔIRS2-1, and ΔIRS2-2 cell line lysates were analyzed for IRS2 expression by immunoblotting.

(B-C) Volcano plots comparing proteomes of ΔIRS2 cell lines with WT cell line. Proteins that significantly decrease > 20% (p-value<0.05) in both cell lines compared to wild-type are shown in purple; proteins that significantly increase > 20% (p-value<0.05) in both cell lines compared to WT are shown in green.

(D) Gene ontology (GO) term enrichment of proteins that decrease in both ΔIRS2 cell lines relative to WT cells.

(E) Heat map depicting cell cycle-related protein abundance changes between ΔIRS2 cell lines and WT cells.

Figure 6: *IRS2 expression promotes a functional spindle assembly checkpoint.*

(A) Mitotic fractional analysis for RPE1 wild type (WT) and IRS2 KO cell lines treated with the indicated doses of nocodazole and S-trityl L-cysteine (STLC) for 18 hours. Mitotic fraction measurements were made using a high content fixed cell imaging assay based on DAPI intensity of stained nuclei. Error bars = mean ± SD.

(B) Asynchronous RPE1 wild type (WT) or IRS2 KO cell lines were treated with 300 nM nocodazole and imaged every five minutes by widefield time lapse microscopy for 36 hours. Each point represents an individual cell's mitotic duration, measured as the time from nuclear envelope breakdown (NEB) to division, slippage, or cell death. Error bars = mean± SD. *p*-values were calculated by one-way ANOVA. **** = $p<0.0001$. ns = not statistically significant.

(C) Asynchronous RPE1 wild type (WT) or IRS2 KO cell lines expressing mAG1-geminin(1-110) were treated as in (C). mAG1 fluorescence intensity was measured from nuclear envelope breakdown (NEB) until division, slippage, or cell death (n=10 for all three cell lines). Error bars = mean ± SEM. Fluorescence intensity was background subtracted and normalized to intensity at NEB.

Figure 7: Model for IRS2's role in cell cycle control. IRS2 is targeted for proteasomal degradation by APC/C^{Cdh1} during G_1. When APC/C is inactivated at the G_1/S boundary, IRS2 protein accumulates, potentially allowing it to stimulate the expression of cell cycle-related proteins either through IR-mediated action (Shirakawa et al., 2017) or through another receptor tyrosine kinase. Some of the proteins that are expressed through this

555 pathway may be required for a robust spindle assembly checkpoint, which directly inhibits
556 APC/C^{Cdc20} during M-phase.
557
558 **Tables**
559 ***Table 1*: 26 proteins containing high-probability D- and KEN-boxes as identified from G_1**
560 **APC/C inhibitor proteomics.**

Gene Symbol	Fold Change	KEN box	D box	Similarity score(s) [a]	Consensus similarity [b]	Disorder Score [c]	Citation [d]
TK1	3.6	Y		0.97	High	0.53	(Ke et al., 2005)
CKAP2	3.2	Y	Y	0.95 ; 0.81	High ; Medium	0.62 ; 0.49	(Seki and Fang, 2007)
KIF11	2.4	Y	Y	0.97 ; 0.84	High ; High	0.57 ; 0.52	(Eguren et al., 2014)
GMNN [e]	2.2	Y	Y	0.80 ; 0.81	Low ; Medium	0.61 ; 0.66	(McGarry and Kirschner, 1998)
TACC3	1.9	Y (2)		0.94/0.90	High/High	0.54/0.49	(Jeng et al., 2009)
TOP2A	1.8	Y		0.86	High	0.44	(Eguren et al., 2014)
MKI67	1.5	Y (2)		0.89/0.86	High/High	0.45/0.48	
CUEDC2	1.4	Y		0.99	High	0.71	(Zhang et al., 2013)
IRS2	1.3		Y	0.87	High	0.68	
GPBP1	1.3	Y		0.81	Medium	0.61	
BUB1B	1.2	Y (2)	Y (2)	0.92/0.85 ; 0.83/0.86	High/Medium ; High/High	0.47/0.64 ; 0.47/0.49	(Choi et al., 2009)
UHRF2	1.2	Y		0.88	High	0.61	
PBXIP1	1.2		Y	0.83	Medium	0.42	(Khumukcham et al., 2019)
DCBLD1	1.2		Y	0.86	High	0.56	
KIF23	1.2	Y		0.87	High	0.45	(Singh et al., 2014)
ULK1	1.2		Y	0.85	High	0.58	
NAA38	1.2		Y	0.82	Medium	0.44	
LRP10	1.2		Y	0.82	Medium	0.49	
PNPLA8	1.2	Y		0.92	High	0.61	
CEP120	1.2		Y	0.84	High	0.42	
DIAPH3 [f]	1.2		Y	0.84	High	0.56	(DeWard and Alberts, 2009)
KDM2A	1.2	Y		0.94	High	0.66	
PRPF38B	1.2	Y		0.92	High	0.44	
DLGAP5	1.2	Y		0.89	High	0.6	(Song and Rape, 2010)
KDM3A	1.2	Y	Y	0.95 ; 0.81	High ; Medium	0.59 ; 0.48	
ANKRD11	1.2		Y	0.86	High	0.53	

Features of the putative degron(s) found in each protein are annotated, including (a) the SLiMSearch similarity score to other validated degrons, (b) the similarity of the surrounding consensus sequence to other validated degrons, (c) the disorder score for the region of the protein in which the degron is located, and (d) the citation of the publication that reports the protein as an APC/C substrate, where applicable. (e) We cannot delineate whether the geminin peptides identified here derive from the FUCCI reporter or the endogenous protein. (f) While DIAPH3/mDia2 has been shown to be ubiquitinated in a cell cycle dependent manner and was suggested as an APC/C substrate, there is no direct cell-based or biochemical evidence for this. Previously reported substrates are shown in bold.

STAR Methods

Cell Culture and Synchronization

All cell lines used in this work (HeLa, C_2C_{12}, hTERT-RPE1-FUCCI, HEK293T) were cultured in a humidified incubator at 37ºC in the presence of 5% CO_2. HeLa, hTERT-RPE1 and C_2C_{12} cells were obtained from American Type Culture Collection (ATCC), and hTERT-RPE1 cells were modified with FUCCI constructs(Sakaue-Sawano et al., 2008) with the permission of the RIKEN Institute. HeLa cells were grown in DMEM with 10% FBS. Proliferating C_2C_{12} myoblasts were grown in DMEM with 15% FBS, whereas differentiated myotubes were cultured in differentiation media, consisting of DMEM with 2% horse serum and 1x insulin, transferrin, selenium (ITS) Premix Universal Culture Supplement (Corning, 354350). hTERT-RPE1-FUCCI cells were grown in DMEM/F12 with 10% FBS supplemented with 0.01 mg/ml hygromycin B (Corning, 30-240-CR). HEK293T cells used for lentivirus generation were a gift from Wade Harper and were cultured in DMEM with 10% FBS. All cell lines tested were negative for mycoplasma contamination (Lonza LT07-218).

HeLa cells were synchronized by double thymidine block by treating with 2 mM thymidine for 18 hours, releasing for 8 hours, and re-treating with 2 mM thymidine for 19 hours. HeLa cells synchronized by thymidine-nocodazole block were treated with 2 mM thymidine for 20 hours, released for 8 hours, then treated with 300-330 nM nocodazole

for 15 hours. Mitotic cells were collected by shake-off and re-plated in drug-free media for cell cycle time course experiments.

RPE1 cells were synchronized by RO3306 treatment by treating with 7.5 μM RO3306 for 18 hours before releasing into fresh media for 30-40 minutes, after which cells were collected by mitotic shake-off and re-plated for cell cycle time course experiments. For G_1 arrest experiments, RPE1 cells were treated with 1 μM palbociclib for 20 hours.

To differentiate C_2C_{12} myoblasts into myotubes, cells were grown to confluence and washed 2x in DMEM with 2% horse serum before switching to differentiation media. Cells were incubated for 72 hours, with media changes every 24-36 hours. Differentiation into myotubes was confirmed visually as well as by immunoblotting for MyoD, a myogenic marker.

Immunoblotting

Cell extracts were prepared in lysis buffer (10 mM Tris HCl pH 7.4, 100 mM NaCl, 1 mM EDTA, 1 mM EGTA, 1 mM NaF, 1 mM PMSF, 20 mM $Na_4P_2O_7$, 2 mM NA_3VO_4, 1% Triton X-100, 10% glycerol, 0.1% SDS, and 0.5% deoxycholate) supplemented with Pierce protease inhibitor tablets (Thermo Fisher Scientific, A32963) and Pierce phosphatase inhibitor tablets (Thermo Fisher Scientific, A32957). Pellets were incubated in lysis buffer on ice for 30 minutes with vortexing and were centrifuged at 13,000rpm for 10 minutes to clear the lysate. Protein concentrations were determined using a bicinchoninic acid (BCA) assay (Thermo Fisher Scientific, 23225). Supernatants were re-suspended in NuPAGE LDS sample buffer (Thermo Fisher Scientific, NP0008) supplemented with 100 mM dithiothreitol (DTT) and boiled at 100ºC for 5 minutes. Equal masses of lysates were separated by SDS-PAGE using either 4-12% Bis Tris gels or 3-8% Tris acetate gels (Thermo Fisher Scientific). All IRS2 immunoblots were separated on 3-8% Tris acetate gels with the exception of those shown in **Figures 5A** and **S4B**, which were separated on 4-12% Bis Tris gels. Proteins were transferred to polyvinylidene difluoride (PVDF) membranes (Thermo Fisher Scientific, 88518).

Membranes were blocked in 5% non-fat dry milk in Tris-buffered saline with 0.1% Tween (TBS-T) before incubating with primary antibodies overnight at 4ºC with agitation. Membranes were probed with secondary antibodies dissolved in 5% milk in TBS-T for 1-2 hours at room temperature before developing with an Amersham 600RGB imaging system. Quantification of immunoblots was done using ImageJ (Schneider et al., 2012).

Antibodies

The following commercially available primary antibodies were used for immunoblotting: anti-IRS2 (Cell Signaling Technologies, 4502) 1:750; anti-Cdh1/Fzr1 (Sigma Aldrich, CC43) 1:500; anti-APC3 (BD Transduction Laboratories, 610455) 1:500; anti-cyclin B1 (Santa Cruz Biotechnology, sc-752) 1:500; anti-Cdc20 (Santa Cruz Biotechnology, sc-8358) 1:500; anti-HA-peroxidase (Sigma Aldrich), 1:1500; anti-cyclin A2 (Santa Cruz Biotechnology, sc-596) 1:500; anti-IRS1 (Cell Signaling Technologies, 2382) 1:750; anti-MyoD1 (Cell Signaling Technologies, 13812) 1:750; anti-GAPDH (Abcam, ab8245) 1:2000; anti-α tubulin (Abcam, ab7291 and Santa Cruz Biotechnology, sc-8035) 1:1000 for both; anti-vinculin (Santa Cruz Biotechnology, sc-73614) 1:2000. Secondary antibodies used: anti-rabbit IgG-HRP (GE Healthcare, NA934) and anti-mouse IgG- HRP (GE Healthcare, NA931V), both at 1:3000 dilutions.

Compounds

The following chemicals were used: palbociclib (LC Laboratories, P-7722), proTAME (Boston Biochem, I-440), MG132 (474790, Calbiochem), S-trityl L-cysteine (STLC, Alfa Aesar, L14384), thymidine (Sigma Aldrich, T9250), nocodazole (Sigma Aldrich, 31430-18-9), RO3306 (AdipoGen Life Sciences, AGCR13515M), doxycycline hyclate (Sigma Aldrich, D9891). Apcin was custom synthesized by Sundia MediTech Company (Lot #A0218-10069-031) using methods described previously (Sackton et al., 2014). All compounds were dissolved in dimethyl sulfoxide (DMSO), with the exception of thymidine and doxycycline, which were dissolved in Dulbecco's phosphate buffered saline (DPBS, Corning, 21-030-CV). Dissolved compounds were stored at -20°C prior to use.

CRISPR/Cas9 mediated gene editing

A TrueGuide crRNA directed against exon 1 of Hs IRS2's coding region (target DNA sequence: 5'- TCG AGA GCG ATC ACC CGT TT -3', Assay ID number: CRISPR850215_CR, Thermo Fisher Scientific) was annealed to the TrueGuide tracrRNA (Thermo Fisher Scientific, A35507) according to manufacturer protocol. hTERT RPE1-FUCCI cells were co-transfected with TrueCut Cas9 protein v2 (Thermo Fisher Scientific, A36496) and the annealed tracrRNA:crRNA complex using the Lipofectamine CRISPRMAX Cas9 Transfection reagent (Thermo Fisher Scientific, CMAX00003) according to manufacturer protocol. Transfected cells were incubated for two days before switching to fresh media and expanding. Single cell clones were isolated using the limiting dilution method in a 96-well format, and clonal cell lines were expanded before screening for knockouts by immunoblotting.

Site directed mutagenesis

R777-E111 Hs.IRS2 and R777-E111 Hs.IRS2-nostop were gifts from Dominic Espositio (Addgene plasmid #70395 and #70396, respectively). Both of these plasmids encode codon optimized sequences for IRS2, with and without a stop codon respectively. R972A mutations were introduced into the aforementioned IRS2 clones using the Q5 Site-Directed Mutagenesis Kit (New England BioLabs) with the primers 5' - AGA TTA TAT GAA TAA GTC CAC TGT CAG ATT ATA TG - 3' and 5' - GAC AGT GGA CTT GCC TGG CGA GAG TCT GAA CT - 3' according to the manufacturer's protocol. For N-terminally FLAG-HA-tagged constructs, the insert from R77-E111 Hs.IRS2 (WT or ΔD) was cloned into the pHAGE-FLAG-HA-NTAP vector (a gift from Wade Harper) using the Gateway LR Clonase II system (Invitrogen). For doxycycline-inducible, C-terminally HA-tagged constructs, the insert from R77-E111 Hs.IRS2-nostop (WT or ΔD) was cloned into pINDUCER20 (a gift from Stephen Elledge, Addgene plasmid #44012) using the Gateway LR Clonase II system (Invitrogen). The ΔD mutation was verified both before and after Gateway cloning by Sanger sequencing.

Lentivirus construction

To construct lentiviruses, HEK293T cells were co-transfected with pPAX2, pMD2, and either pINDUCER-20-IRS2 or pHAGE-FLAG-HA-NTAP-IRS2 in a 4:2:1 DNA ratio using

Lipofectamine 3000 (Invitrogen, L3000001) according to manufacturer's instructions. pPAX2 and pMD2 were gifts from Wade Harper. 24 hours after transfection, HEK293T cells were switched to fresh media (DMEM + 10% FBS). 48 hours after transfection lentiviruses were harvested by clearing debris by centrifugation at 960*xg* for 5 minutes and filtering through 0.45 µm SFCA filters. Lentiviruses were either used immediately or flash frozen in liquid nitrogen and stored at -80ºC for later use.

Stable cell line construction

To generate stable cell lines, plated HeLa, RPE1, or C_2C_{12} cells were incubated with lentiviruses and 2 µg/ml protamine sulfate. 24 hours after viral infection, cells were switched to fresh media. 48 hours after viral infection, antibiotics were introduced. For lentiviruses derived from pINDUCER20, geneticin (Invitrogen, 10131027) was used at a concentration of 750 µg/ml for both RPE1 and C_2C_{12} for 6-7 days. For lentiviruses derived from pHAGE-FLAG-HA-NTAP, puromycin (Sigma Aldrich, P8833) was used at a concentration of 0.5 µg/ml for 3 days. Antibiotic-selected populations of cells were expanded and used for further experiments without clonal selection.

Small interfering RNAs (siRNAs)

Cells were transfected using RNAiMax (Invitrogen, 13778100) according to manufacturer's instructions with the following siRNAs: siGENOME Non-Targeting Control siRNA #5 (D-001210-05, Dharmacon); ON-TARGETplus Human FZR1 siRNA (J-015377-08, Dharmacon), 25 nM; SMARTpool ON-TARGETplus Mouse Fzr1 siRNA (L-065289-01-0005), 25 nM. Cells were treated with siRNAs for 24 hours for all experiments. For experiments involving subsequent compound treatment, cells were switched to fresh media prior to the addition of compounds.

Plasmid transfection

C_2C_{12} myoblasts were transfected with a plasmid containing the N-terminal 88 amino acids of human cyclin B1 fused to EGFP using Lipofectamine 3000 (Invitrogen, L3000001) with the P3000 reagent according to manufacturer's instructions. Growth

media was refreshed to remove transfection reagents 24 hours post-transfection, and cells were switched to differentiation media for an additional 3 days.

Time lapse and fluorescence microscopy

Cells were plated in a 24-well coverslip-bottom plate (Greiner BioOne, 662892). After 24 hours, cells were treated with the indicated compounds and were imaged immediately afterwards. Plates were inserted into a covered cage microscope incubator (OkoLab) with temperature and humidity control at 37ºC and 5% CO_2 and mounted on a motorized microscope stage (Prior ProScan III). All images were collected on a Nikon Ti motorized inverted microscope equipped with a 20x/0.75 NA Plan Apo objective lens and the Perfect Focus system. mCherry fluorescence was excited with a Lumencor Spectra-X using a 555/25 excitation filter and a 605/52 emission filter (Chroma). mAG1 fluorescence was excited using a 490/20 excitation filter and a 525/36 emission filter (Chroma). Both configurations used a Sedat Quad dichroic (Chroma). Images were acquired with a Hamamatsu Orca-R2 or Hamamatsu Flash 4.0 V2 controlled with Nikon Elements image acquisition software. Three fields of view were collected per condition, and phase contrast and/or fluorescence images were captured at 5- to 8-minute intervals (depending upon the experiment) for 24-48 hours.

Videos were analyzed using ImageJ. Mitotic duration was defined as the time from nuclear envelope breakdown (NEB) until division, death (cytoplasmic blebbing), or mitotic slippage. mAG1 and mCherry intensities were quantified manually by measuring the maximum intensity of signal for each cell in a given frame across multiple time points. For experiments analyzing fluorescence intensity during G_1 arrest, measurements were made for all cells in a frame for each time point.

TMT mass spectrometry sample preparation

Cells were cultured as described in biological triplicate. Cells pellets were re-suspended in urea lysis buffer: 8M urea, 200 mM EPPS pH 8.0, Pierce protease inhibitor tablets (Thermo Fisher Scientific, A32963), and Pierce phosphatase inhibitor tablets (Thermo Fisher Scientific, A32957). Lysates were passed through a 21-gauge needle 20 times,

and protein concentrations were measured by BCA assay (Thermo Fisher Scientific). 100 µg of protein were reduced with 5 mM tris-2-carboxyethyl-phosphine (TCEP) at room temperature for 15 minutes, alkylated with 10 mM iodoacetamide at room temperature for 30 minutes in the dark, and were further reduced with 15 mM DTT for 15 minutes at room temperature. Proteins were precipitated using a methanol/chloroform extraction. Pelleted proteins were resuspended in 100 µL 200 mM EPPS, pH 8.0. LysC (Wako, 125-05061) was added at a 1:50 enzyme:protein ratio, and samples were incubated overnight at room temperature with agitation. Following overnight incubation, trypsin (Promega, V5111) was added at a 1:100 enzyme:protein ratio, and samples were incubated for an additional 6 hours at 37ºC. Tryptic digestion was halted by the addition of acetonitrile (ACN). Tandem mass tag (TMT) isobaric reagents (Thermo Fisher Scientific, 90406) were dissolved in anhydrous ACN to a final concentration of 20 mg/mL, of which a unique TMT label was added at a 2:1 label:peptide ratio. Peptides were incubated at room temperature for one hour with vortexing after 30 minutes. TMT labeling reactions were quenched by the addition of 10 µL of 5% hydroxylamine. Equal amounts of each sample were combined at a 1:1 ratio across all channels and lyophilized by vacuum centrifugation. Samples were re-suspended in 1% formic acid (FA)/99% water and were desalted using a 50 mg 1cc SepPak C18 cartridge (Waters, WAT054955) under vacuum. Peptides were eluted with 70% ACN/1% FA and lyophilized to dryness by vacuum centrifugation. The combined peptides were fractionated with basic pH reversed-phase (BPRP) HPLC, collected in a 96-well format and consolidated to a final of 24 fractions, out of which only alternating fractions (a total of 12) were analyzed (Navarrete-Perea et al., 2018). Each fraction was desalted via StageTip, lyophilized to dryness by vacuum centrifugation, and reconstituted in 5% ACN/5% FA for LC-MS/MS processing.

TMT mass spectrometry analysis

Data for the G_1 APC inhibition experiment were collected on an Orbitrap Fusion mass spectrometer coupled to a Proxeon EASY-nLC 1000 liquid chromatography (LC) pump (Thermo Fisher Scientific), whereas data for IRS2 knockout cell line analysis were collected on an Orbitrap Fusion Lumos mass spectrometer coupled to a Proxeon EASY-nLC 1200 liquid chromatography (LC) pump. The 100 µm capillary column was packed

with 30 cm of Accucore 150 resin (2.6 µm, 150Å; Thermo Fisher Scientific). Mobile phases were 5% ACN, 0.125% FA (Buffer A) and 95% ACN, 0.125% FA (Buffer B). Peptides from G_1 APC inhibition experiment were separated using a 2.5 h gradient from 4% to 26% Buffer B and analyzed with a SPS-MS3 method (McAlister et al., 2014). Peptides from IRS2 knockout cell line analysis were separated using a 2 h gradient from 4% to 30% Buffer B and analyzed with a real-time search strategy (Erickson et al., 2019; Schweppe et al., 2019).

Raw data were converted to mzXML format using a modified version of RawFileReader and searched against a human protein target-decoy database. Searches were performed with a 50 ppm precursor mass tolerance, 0.9 Da fragment mass tolerance, trypsin digest with up to 2 missed cleavages. Allowed modifications include cysteine carboxyamidomethylation (+57.02146), static TMT on lysine and peptide N-temini (+229.16293) and up to 3 variable methionine oxidation (+15.99491). Peptide spectral matches were filtered with a linear discriminant analysis (LDA) method to a 1% FDR (Huttlin et al., 2010) and a protein-level FDR of 1% was also implemented (Savitski et al., 2015). For peptide quantification, we extracted the TMT signal-to-noise and column normalized each channel to correct for equal protein loading. Peptide spectral matches with summed signal-to-noise less than 100 were excluded from final result. Lastly, each protein was scaled such that the summed signal-to-noise for that protein across all channels equals 100, thereby generating a relative abundance (RA) measurement.

High content mitotic fraction assay

Asynchronous hTERT RPE1-FUCCI wild-type or IRS2 KO cell lines were plated in a black, clear-bottom 96-well plate (Corning, 3606). Plates were sealed with breathable white rayon sealing tape (Nunc, 241205) to prevent evaporation following plating and during all subsequent incubations. In experiments involving RNAi, cells were treated with siRNAs for 24 hours. Cells were switched to fresh media, and compounds were added at the indicated concentrations for an additional 18 hours. Following compound treatment, cells were fixed and stained directly without additional washing steps (to avoid the loss of loosely attached mitotic cells) with 10% formalin, 0.33 µg/mL Hoechst 33342, and 0.1%

Triton X-100 in DPBS. Plates were sealed with aluminum tape (Nunc, 276014) and were incubated for 45 minutes room temperature in the dark before imaging. All experimental conditions were represented in triplicate on the same plate. Plates were imaged using an ImageXpress Micro high-content microscope (Molecular Devices) equipped with a 10x objective lens. Four images were acquired per well, yielding a total of 12 images per conditions. Images were processed automatically in ImageJ to identify and count nuclei as well as measure their maximum fluorescence intensity. ImageJ output files were pooled, and cumulative frequency curves for the maximum intensity of the cell population in each condition were computed using MATLAB. An intensity threshold was set based on the intensity of mitotic cells in control (DMSO-treated) wells to delineate interphase cells from mitotic cells. The fraction of mitotic cells was calculated as the fraction of cells above the set intensity threshold in MATLAB(Sackton et al., 2014).

Statistical analyses

For experiments regarding the stability of IRS2-WT and IRS2-ΔD, *p*-values were calculated by two-way ANOVA. For fluorescence microscopy experiments that quantify mAG1 intensity in response to drug treatment over time, *p*-values were calculated by two-way ANOVA. For microscopy experiments that quantify mitotic duration following nocodazole treatment, *p*-values were calculated by one-way ANOVA. For proteomics data, *p*-values were calculated using a two-tailed, unpaired Student's t-test. For time lapse microscopy data, *p*-values were calculated by one-way ANOVA. Gene enrichment was calculated using the AmiGO 2 search tool (Carbon et al., 2009). Error bars indicate standard deviation (SD) or standard error of the mean (SEM) where indicated.

Materials Availability

All mass spectrometry raw files will be available through the PRIDE archive upon publication. All other data are available in the associated supplementary data files. Further information and requests for resources and reagents should be directed to the Lead Contact, Randy King (randy_king@hms.harvard.edu).

Supplemental Information Legends

Figure S1: *Related to Figure 1*

(A) Asynchronous RPE1 cells were treated with 1 μM palbociclib and imaged by fluorescence time lapse microscopy for 20 hours. Frames at 0, 10, and 20 hours are shown.

(B) From the experiment shown in Figure S1B, FITC intensity was quantified at 0 hours (time of drug addition) and 20 hours. Each point represents the maximum FITC intensity of an individual cell at the given time point. ns : not significant ; **** : $p<0.0001$.

(C) Asynchronous RPE1 cells were treated with 1 μM palbociclib for 20 hours. Following G_1 arrest, cells were treated with either DMSO or APC inhibitors (6 μM proTAME + 50 μM apcin) and imaged by fluorescence widefield time lapse microscopy for an additional eight hours.

(D) Quantification of the experiment shown in S1D, as explained in S1B. Error bars = SD among all of the cells quantified for each condition. ns: not significant ; **** : $p<0.0001$.

Figure S2: *Related to Figure 2B*

(A) Asynchronous C_2C_{12} myoblasts and 3-day differentiated C_2C_{12} myotubes were lysed and MyoD levels were measured by immunoblotting.

(B) Phase-contrast images of asynchronous (Day 0) C_2C_{12} myoblasts and 3-day differentiated C_2C_{12} myotubes.

(C) Asynchronous C_2C_{12} myoblasts were transfected with a plasmid coding for the N-terminal fragment of cyclin B1 (amino acids 1-88) fused to EGFP for 24 hours. Following transfection, cells were switched to low-serum differentiation media containing ITS for three days with media refreshment every 24 hours. After 3 days, myotubes were acutely treated with either DMSO or APC inhibitors (6 μM proTAME + 50 μM apcin) for an additional 8 hours. Myotubes were then harvested, and lysates were analyzed for transgene expression by immunoblot.

Figure S3: *Related to Figure 3*

(D) HeLa cells were synchronized by double thymidine block and released into S-phase either in the presence of DMSO or 5 μM RO3306. Cells were harvested at the

870 indicated time points for analysis of the given protein abundances and phosphorylation
871 patterns in lysate by immunoblot.
872
873 ***Figure S4***: *Related to Figure 4*
874 (A) *(left)* RPE1 cells stably expressing lentivirus generated, C-terminally HA-tagged IRS2
875 wild type (WT) and R972A (ΔD) constructs were arrested in G_1 with 1 μM palbociclib
876 for 20 hours. Cells were then acutely treated with either DMSO or the indicated dose
877 range of APC inhibitors for an additional 8 hours. Cells were then harvested, and
878 lysate was analyzed for HA expression by immunoblot. The lane denoted t_0 indicates
879 a sample that was collected at the time of drug addition. (*right*) The experiment shown
880 at left was repeated three times, and HA intensity was quantified. Plot shows HA
881 intensity normalized to a loading control (either GAPDH or Ponceau) and to the DMSO
882 condition. Error bars = mean ± SEM.
883 (B) (*top*) Asynchronous RPE1 cells expressing doxycycline-inducible, C-terminally HA
884 tagged IRS2 variants were treated with a dose range of doxycycline. HA and IRS2
885 expression levels were analyzed by immunoblotting cell lysates. Red = doxycycline
886 dose used for all experiments. (*bottom*) Asynchronous C_2C_{12} cells expressing
887 doxycycline-inducible, C-terminally HA tagged IRS2 variants were treated with a dose
888 range of doxycycline. HA and IRS2 expression levels were analyzed by
889 immunoblotting cell lysates. Red = doxycycline dose used for all experiments.
890
891 ***Figure S5***: *Related to Figure 5*
892 (A) Hierarchical clustering for the nine conditions analyzed by TMT-coupled quantitative
893 mass spectrometry in wild type and ΔIRS2 cell lines.
894 (B) Venn diagrams depicting proteins that (*left*) decrease significantly >20% relative to
895 WT cells in both ΔIRS2 cell lines and (*right*) increase significantly >20% relative to WT
896 in both ΔIRS2 cell lines.
897 (C) Gene ontology (GO) term enrichment of proteins that increase in both ΔIRS2 cell lines
898 relative to WT cells.

(D) Fraction abundance of cell-cycle related proteins shown in Figure 5D depleted in ΔIRS2 cell lines relative to WT cells. ΔIRS2-1 median abundance = 0.70 ; ΔIRS2-2 median abundance = 0.66.

Figure S6: *Related to Figure 6*

(A) Representative frames from high-content nuclear imaging experiment for mitotic fraction based on DAPI intensity. Asynchronous RPE1 WT or IRS2 KO cell lines were treated with 900 nM nocodazole for 18 hours before fixing and DAPI staining.

(B) Asynchronous RPE1 WT or IRS2 KO cell lines were imaged every five minutes by widefield time lapse microscopy for 36 hours. Each point represents an individual cell's mitotic duration, measured as the time from nuclear envelope breakdown (NEB) to division, slippage, or cell death. Error bars = mean ± SD. *p*-values were calculated using one-way ANOVA. ns = not statistically significant.

Figure S7: *Related to Figures 1-3*

Extended immunoblots from Figures 1, 2, and 3

Figure S8: *Related to Figures 4-5*

Extended immunoblots from Figures 4 and 5.

Table S1: APC inhibition in G_1 proteomics

Table S2: Reported APC/C substrates identified by proteomics

Table S3: 204 protein subset

Table S4: IRS2 knockout cell proteomics

References

Alfieri, C., Zhang, S., and Barford, D. (2017). Visualizing the complex functions and mechanisms of the anaphase promoting complex/cyclosome (APC/C). Open Biol *7*.

Besse-Patin, A., Jeromson, S., Levesque-Damphousse, P., Secco, B., Laplante, M., and Estall, J.L. (2019). PGC1A regulates the IRS1:IRS2 ratio during fasting to influence hepatic metabolism downstream of insulin. Proc Natl Acad Sci U S A *116*, 4285-4290.

Bouzakri, K., Zachrisson, A., Al-Khalili, L., Zhang, B.B., Koistinen, H.A., Krook, A., and Zierath, J.R. (2006). siRNA-based gene silencing reveals specialized roles of IRS-1/Akt2 and IRS-2/Akt1 in glucose and lipid metabolism in human skeletal muscle. Cell Metab *4*, 89-96.

Carbon, S., Ireland, A., Mungall, C.J., Shu, S., Marshall, B., Lewis, S., Ami, G.O.H., and Web Presence Working, G. (2009). AmiGO: online access to ontology and annotation data. Bioinformatics *25*, 288-289.

Chang, L., and Barford, D. (2014). Insights into the anaphase-promoting complex: a molecular machine that regulates mitosis. Curr Opin Struct Biol *29*, 1-9.

Chen, L., Li, Z., Ahmad, N., and Liu, X. (2015). Plk1 phosphorylation of IRS2 prevents premature mitotic exit via AKT inactivation. Biochemistry *54*, 2473-2480.

Chirivella, L., Kirstein, M., Ferron, S.R., Domingo-Muelas, A., Durupt, F.C., Acosta-Umanzor, C., Cano-Jaimez, M., Perez-Sanchez, F., Barbacid, M., Ortega, S.*, et al.* (2017). Cyclin-Dependent Kinase 4 Regulates Adult Neural Stem Cell Proliferation and Differentiation in Response to Insulin. Stem Cells *35*, 2403-2416.

Choi, B.H., Pagano, M., Huang, C., and Dai, W. (2014). Cdh1, a substrate-recruiting component of anaphase-promoting complex/cyclosome (APC/C) ubiquitin E3 ligase, specifically interacts with phosphatase and tensin homolog (PTEN) and promotes its removal from chromatin. J Biol Chem *289*, 17951-17959.

Choi, E., Choe, H., Min, J., Choi, J.Y., Kim, J., and Lee, H. (2009). BubR1 acetylation at prometaphase is required for modulating APC/C activity and timing of mitosis. EMBO J *28*, 2077-2089.

Choi, E., Kikuchi, S., Gao, H., Brodzik, K., Nassour, I., Yopp, A., Singal, A.G., Zhu, H., and Yu, H. (2019). Mitotic regulators and the SHP2-MAPK pathway promote IR endocytosis and feedback regulation of insulin signaling. Nature Communications *10*, 1473.

Choi, E., Zhang, X., Xing, C., and Yu, H. (2016). Mitotic Checkpoint Regulators Control Insulin Signaling and Metabolic Homeostasis. Cell *166*, 567-581.

Clijsters, L., Ogink, J., and Wolthuis, R. (2013). The spindle checkpoint, APC/C(Cdc20), and APC/C(Cdh1) play distinct roles in connecting mitosis to S phase. J Cell Biol *201*, 1013-1026.

Copps, K.D., and White, M.F. (2012). Regulation of insulin sensitivity by serine/threonine phosphorylation of insulin receptor substrate proteins IRS1 and IRS2. Diabetologia *55*, 2565-2582.

Davey, N.E., and Morgan, D.O. (2016). Building a Regulatory Network with Short Linear Sequence Motifs: Lessons from the Degrons of the Anaphase-Promoting Complex. Mol Cell *64*, 12-23.

DeWard, A.D., and Alberts, A.S. (2009). Ubiquitin-mediated degradation of the formin mDia2 upon completion of cell division. J Biol Chem *284*, 20061-20069.

Eguren, M., Alvarez-Fernandez, M., Garcia, F., Lopez-Contreras, A.J., Fujimitsu, K., Yaguchi, H., Luque-Garcia, J.L., Fernandez-Capetillo, O., Munoz, J., Yamano, H.*, et al.* (2014). A synthetic lethal interaction between APC/C and topoisomerase poisons uncovered by proteomic screens. Cell Rep *6*, 670-683.

980 Erickson, B.K., Mintseris, J., Schweppe, D.K., Navarrete-Perea, J., Erickson, A.R.,
981 Nusinow, D.P., Paulo, J.A., and Gygi, S.P. (2019). Active Instrument Engagement
982 Combined with a Real-Time Database Search for Improved Performance of Sample
983 Multiplexing Workflows. J Proteome Res *18*, 1299-1306.

984 Ezhevsky, S.A., Nagahara, H., Vocero-Akbani, A.M., Gius, D.R., Wei, M.C., and Dowdy,
985 S.F. (1997). Hypo-phosphorylation of the retinoblastoma protein (pRb) by cyclin D:Cdk4/6
986 complexes results in active pRb. Proc Natl Acad Sci U S A *94*, 10699-10704.

987 Folli, F., Okada, T., Perego, C., Gunton, J., Liew, C.W., Akiyama, M., D'Amico, A., La
988 Rosa, S., Placidi, C., Lupi, R.*, et al.* (2011). Altered insulin receptor signalling and beta-
989 cell cycle dynamics in type 2 diabetes mellitus. PLoS One *6*, e28050.

990 Glotzer, M., Murray, A.W., and Kirschner, M.W. (1991). Cyclin is degraded by the ubiquitin
991 pathway. Nature *349*, 132-138.

992 Haeusler, R.A., McGraw, T.E., and Accili, D. (2017). Biochemical and cellular properties
993 of insulin receptor signalling. Nature Reviews Molecular Cell Biology *19*, 31.

994 Holt, L.J. (2012). Regulatory modules: Coupling protein stability to phopshoregulation
995 during cell division. FEBS Lett *586*, 2773-2777.

996 Hornbeck, P.V., Zhang, B., Murray, B., Kornhauser, J.M., Latham, V., and Skrzypek, E.
997 (2015). PhosphoSitePlus, 2014: mutations, PTMs and recalibrations. Nucleic Acids Res
998 *43*, D512-520.

999 Huttlin, E.L., Jedrychowski, M.P., Elias, J.E., Goswami, T., Rad, R., Beausoleil, S.A.,
1000 Villen, J., Haas, W., Sowa, M.E., and Gygi, S.P. (2010). A tissue-specific atlas of mouse
1001 protein phosphorylation and expression. Cell *143*, 1174-1189.

1002 Jeng, J.C., Lin, Y.M., Lin, C.H., and Shih, H.M. (2009). Cdh1 controls the stability of
1003 TACC3. Cell Cycle *8*, 3537-3544.

1004 Ke, P.Y., Kuo, Y.Y., Hu, C.M., and Chang, Z.F. (2005). Control of dTTP pool size by
1005 anaphase promoting complex/cyclosome is essential for the maintenance of genetic
1006 stability. Genes Dev *19*, 1920-1933.

1007 Khumukcham, S.S., Samanthapudi, V.S.K., Penugurti, V., Kumari, A., Kesavan, P.S.,
1008 Velatooru, L.R., Kotla, S.R., Mazumder, A., and Manavathi, B. (2019). Hematopoietic
1009 PBX-interacting protein is a substrate and an inhibitor of the APC/C-Cdc20 complex and
1010 regulates mitosis by stabilizing cyclin B1. J Biol Chem *294*, 10236-10252.

1011 Klitzing, C., Huss, R., Illert, A.L., Froschl, A., Wotzel, S., Peschel, C., Bassermann, F.,
1012 and Duyster, J. (2011). APC/C(Cdh1)-mediated degradation of the F-box protein NIPA is
1013 regulated by its association with Skp1. PLoS One *6*, e28998.

1014 Krystkowiak, I., and Davey, N.E. (2017). SLiMSearch: a framework for proteome-wide
1015 discovery and annotation of functional modules in intrinsically disordered regions. Nucleic
1016 Acids Res *45*, W464-W469.

1017 Kubota, N., Kubota, T., Itoh, S., Kumagai, H., Kozono, H., Takamoto, I., Mineyama, T.,
1018 Ogata, H., Tokuyama, K., Ohsugi, M.*, et al.* (2008). Dynamic functional relay between
1019 insulin receptor substrate 1 and 2 in hepatic insulin signaling during fasting and feeding.
1020 Cell Metab *8*, 49-64.

1021 Lavin, D.P., White, M.F., and Brazil, D.P. (2016). IRS proteins and diabetic complications.
1022 Diabetologia *59*, 2280-2291.

1023 Lei, L., Han, F., Cui, Q., Liao, W., Liu, H., Guan, G., and Yang, L. (2018). IRS2 depletion
1024 inhibits cell proliferation and decreases hormone secretion in mouse granulosa cells. J
1025 Reprod Dev *64*, 409-416.

1026 Long, Y.C., Cheng, Z., Copps, K.D., and White, M.F. (2011). Insulin receptor substrates
1027 Irs1 and Irs2 coordinate skeletal muscle growth and metabolism via the Akt and AMPK
1028 pathways. Mol Cell Biol *31*, 430-441.

1029 Mailand, N., and Diffley, J.F. (2005). CDKs promote DNA replication origin licensing in
1030 human cells by protecting Cdc6 from APC/C-dependent proteolysis. Cell *122*, 915-926.

1031 McAlister, G.C., Nusinow, D.P., Jedrychowski, M.P., Wuhr, M., Huttlin, E.L., Erickson,
1032 B.K., Rad, R., Haas, W., and Gygi, S.P. (2014). MultiNotch MS3 enables accurate,
1033 sensitive, and multiplexed detection of differential expression across cancer cell line
1034 proteomes. Anal Chem *86*, 7150-7158.

1035 McGarry, T.J., and Kirschner, M.W. (1998). Geminin, an Inhibitor of DNA Replication, Is
1036 Degraded during Mitosis. Cell *93*, 1043-1053.

1037 Nakao, R., Hirasaka, K., Goto, J., Ishidoh, K., Yamada, C., Ohno, A., Okumura, Y.,
1038 Nonaka, I., Yasutomo, K., Baldwin, K.M.*, et al.* (2009). Ubiquitin ligase Cbl-b is a negative
1039 regulator for insulin-like growth factor 1 signaling during muscle atrophy caused by
1040 unloading. Mol Cell Biol *29*, 4798-4811.

1041 Navarrete-Perea, J., Yu, Q., Gygi, S.P., and Paulo, J.A. (2018). Streamlined Tandem
1042 Mass Tag (SL-TMT) Protocol: An Efficient Strategy for Quantitative (Phospho)proteome
1043 Profiling Using Tandem Mass Tag-Synchronous Precursor Selection-MS3. J Proteome
1044 Res *17*, 2226-2236.

1045 Prinz, S., Hwang, E.S., Visintin, R., and Amon, A. (1998). The regulation of Cdc20
1046 proteolysis reveals a role for the APC components Cdc23 and Cdc27 during S phase and
1047 early mitosis. Current Biology *8*, 750-760.

1048 Puklowski, A., Homsi, Y., Keller, D., May, M., Chauhan, S., Kossatz, U., Grunwald, V.,
1049 Kubicka, S., Pich, A., Manns, M.P.*, et al.* (2011). The SCF-FBXW5 E3-ubiquitin ligase is
1050 regulated by PLK4 and targets HsSAS-6 to control centrosome duplication. Nat Cell Biol
1051 *13*, 1004-1009.

1052 Rui, L., Yuan, M., Frantz, D., Shoelson, S., and White, M.F. (2002). SOCS-1 and SOCS-
1053 3 block insulin signaling by ubiquitin-mediated degradation of IRS1 and IRS2. J Biol Chem
1054 *277*, 42394-42398.

1055 Sackton, K.L., Dimova, N., Zeng, X., Tian, W., Zhang, M., Sackton, T.B., Meaders, J.,
1056 Pfaff, K.L., Sigoillot, F., Yu, H.*, et al.* (2014). Synergistic blockade of mitotic exit by two
1057 chemical inhibitors of the APC/C. Nature *514*, 646-649.

1058 Sakaue-Sawano, A., Kurokawa, H., Morimura, T., Hanyu, A., Hama, H., Osawa, H.,
1059 Kashiwagi, S., Fukami, K., Miyata, T., Miyoshi, H.*, et al.* (2008). Visualizing
1060 spatiotemporal dynamics of multicellular cell-cycle progression. Cell *132*, 487-498.

1061 Savitski, M.M., Wilhelm, M., Hahne, H., Kuster, B., and Bantscheff, M. (2015). A Scalable
1062 Approach for Protein False Discovery Rate Estimation in Large Proteomic Data Sets. Mol
1063 Cell Proteomics *14*, 2394-2404.

1064 Scheufele, F., Wolf, B., Kruse, M., Hartmann, T., Lempart, J., Muhlich, S., Pfeiffer, A.F.H.,
1065 Field, L.J., Charron, M.J., Pan, Z.Q.*, et al.* (2014). Evidence for a regulatory role of Cullin-
1066 RING E3 ubiquitin ligase 7 in insulin signaling. Cell Signal *26*, 233-239.

1067 Schneider, C.A., Rasband, W.S., and Eliceiri, K.W. (2012). NIH Image to ImageJ: 25
1068 years of image analysis. Nature Methods *9*, 671-675.

1069 Schweppe, D.K., Eng, J.K., Bailey, D., Rad, R., Yu, Q., Navarrete-Perea, J., Huttlin, E.L.,
1070 Erickson, B.K., Paulo, J.A., and Gygi, S.P. (2019).

1071 Seki, A., and Fang, G. (2007). CKAP2 is a spindle-associated protein degraded by
1072 APC/C-Cdh1 during mitotic exit. J Biol Chem *282*, 15103-15113.

1073 Shi, J., Luo, L., Eash, J., Ibebunjo, C., and Glass, D.J. (2011). The SCF-Fbxo40 complex
1074 induces IRS1 ubiquitination in skeletal muscle, limiting IGF1 signaling. Dev Cell *21*, 835-
1075 847.

1076 Shirakawa, J., Fernandez, M., Takatani, T., El Ouaamari, A., Jungtrakoon, P., Okawa,
1077 E.R., Zhang, W., Yi, P., Doria, A., and Kulkarni, R.N. (2017). Insulin Signaling Regulates
1078 the FoxM1/PLK1/CENP-A Pathway to Promote Adaptive Pancreatic beta Cell
1079 Proliferation. Cell Metab *25*, 868-882 e865.

1080 Singh, S.A., Winter, D., Kirchner, M., Chauhan, R., Ahmed, S., Ozlu, N., Tzur, A., Steen,
1081 J.A., and Steen, H. (2014). Co-regulation proteomics reveals substrates and mechanisms
1082 of APC/C-dependent degradation. EMBO J *33*, 385-399.

1083 Song, L., and Rape, M. (2010). Regulated degradation of spindle assembly factors by the
1084 anaphase-promoting complex. Mol Cell *38*, 369-382.

1085 Song, M.S., Carracedo, A., Salmena, L., Song, S.J., Egia, A., Malumbres, M., and
1086 Pandolfi, P.P. (2011). Nuclear PTEN regulates the APC-CDH1 tumor-suppressive
1087 complex in a phosphatase-independent manner. Cell *144*, 187-199.

1088 Sun, X.J., Wang, L.M., Zhang, Y., Yenush, L., Myers, M.G., Jr., Glasheen, E., Lane, W.S.,
1089 Pierce, J.H., and White, M.F. (1995). Role of IRS-2 in insulin and cytokine signalling.
1090 Nature *377*, 173-177.

1091 Wan, Y., Liu, X., and Kirschner, M.W. (2001). The Anaphase-Promoting Complex
1092 Mediates TGF-β Signaling by Targeting SnoN for Destruction. Molecular Cell *8*, 1027-
1093 1039.

1094 Wang, H., Liu, D., Wang, Y., Qin, J., and Elledge, S.J. (2001). Pds1 phosphorylation in
1095 response to DNA damage is essential for its DNA damage checkpoint function. Genes
1096 Dev *15*, 1361-1372.

1097 Wu, S., Zhou, B., Xu, L., and Sun, H. (2009). IRS-2, but not IRS-1, can sustain
1098 proliferation and rescue UBF stabilization in InR or InR defective signaling of 32D myeloid
1099 cells. Cell Cycle *8*, 3218-3226.

Xu, X., Sarikas, A., Dias-Santagata, D.C., Dolios, G., Lafontant, P.J., Tsai, S.C., Zhu, W., Nakajima, H., Nakajima, H.O., Field, L.J., *et al.* (2008). The CUL7 E3 ubiquitin ligase targets insulin receptor substrate 1 for ubiquitin-dependent degradation. Mol Cell *30*, 403-414.

Yi, J.S., Park, J.S., Ham, Y.M., Nguyen, N., Lee, N.R., Hong, J., Kim, B.W., Lee, H., Lee, C.S., Jeong, B.C., *et al.* (2013). MG53-induced IRS-1 ubiquitination negatively regulates skeletal myogenesis and insulin signalling. Nat Commun *4*, 2354.

Zeng, X., Sigoillot, F., Gaur, S., Choi, S., Pfaff, K.L., Oh, D.C., Hathaway, N., Dimova, N., Cuny, G.D., and King, R.W. (2010). Pharmacologic inhibition of the anaphase-promoting complex induces a spindle checkpoint-dependent mitotic arrest in the absence of spindle damage. Cancer Cell *18*, 382-395.

Zhang, P.J., Zhao, J., Li, H.Y., Man, J.H., He, K., Zhou, T., Pan, X., Li, A.L., Gong, W.L., Jin, B.F., *et al.* (2007). CUE domain containing 2 regulates degradation of progesterone receptor by ubiquitin-proteasome. EMBO J *26*, 1831-1842.

Zhang, W.N., Zhou, J., Zhou, T., Li, A.L., Wang, N., Xu, J.J., Chang, Y., Man, J.H., Pan, X., Li, T., *et al.* (2013). Phosphorylation-triggered CUEDC2 degradation promotes UV-induced G1 arrest through APC/C(Cdh1) regulation. Proc Natl Acad Sci U S A *110*, 11017-11022.

Figure 1

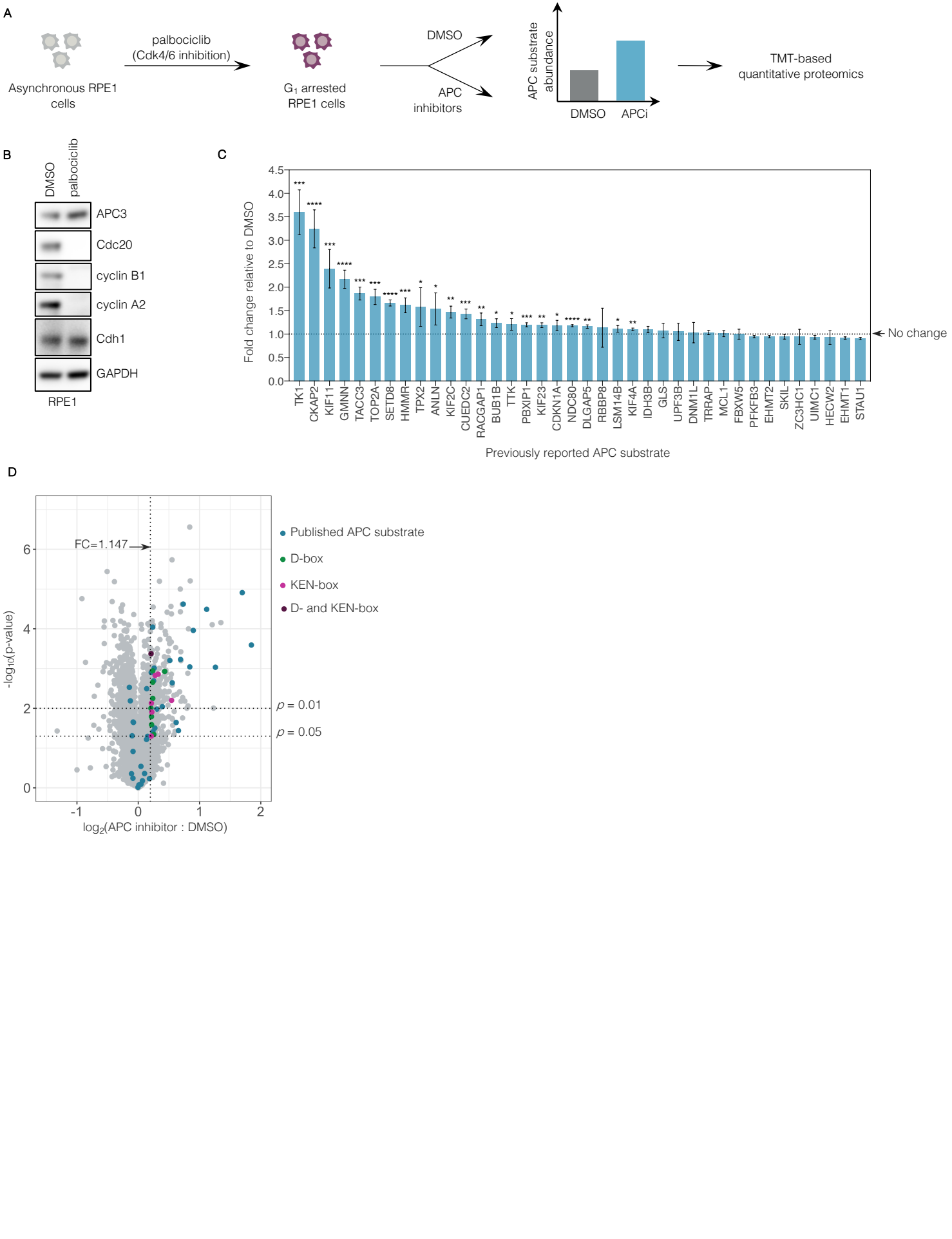

Figure 2

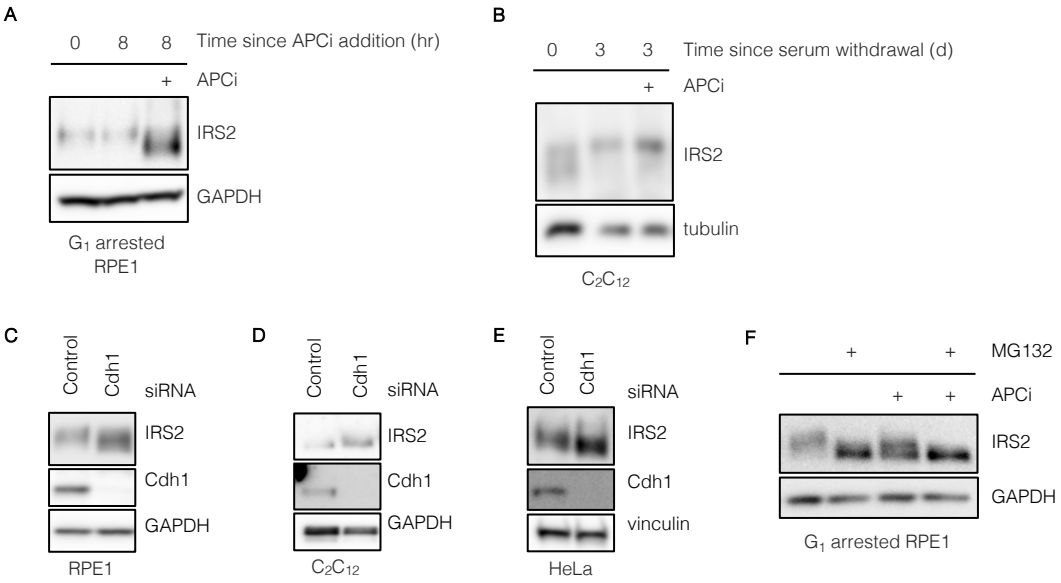

Figure 3

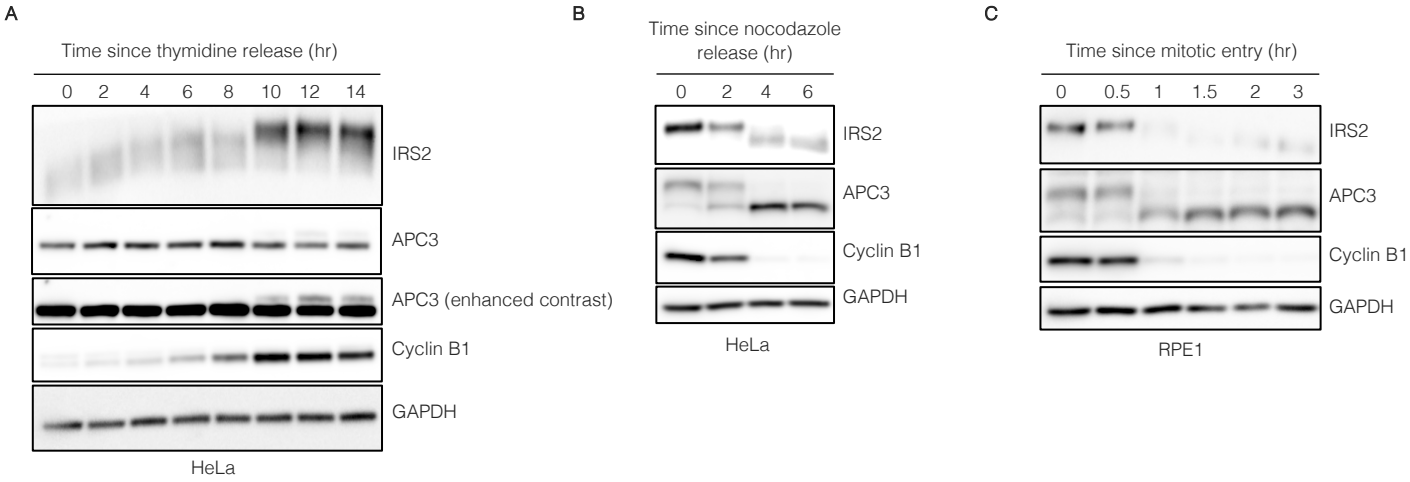

Figure 4

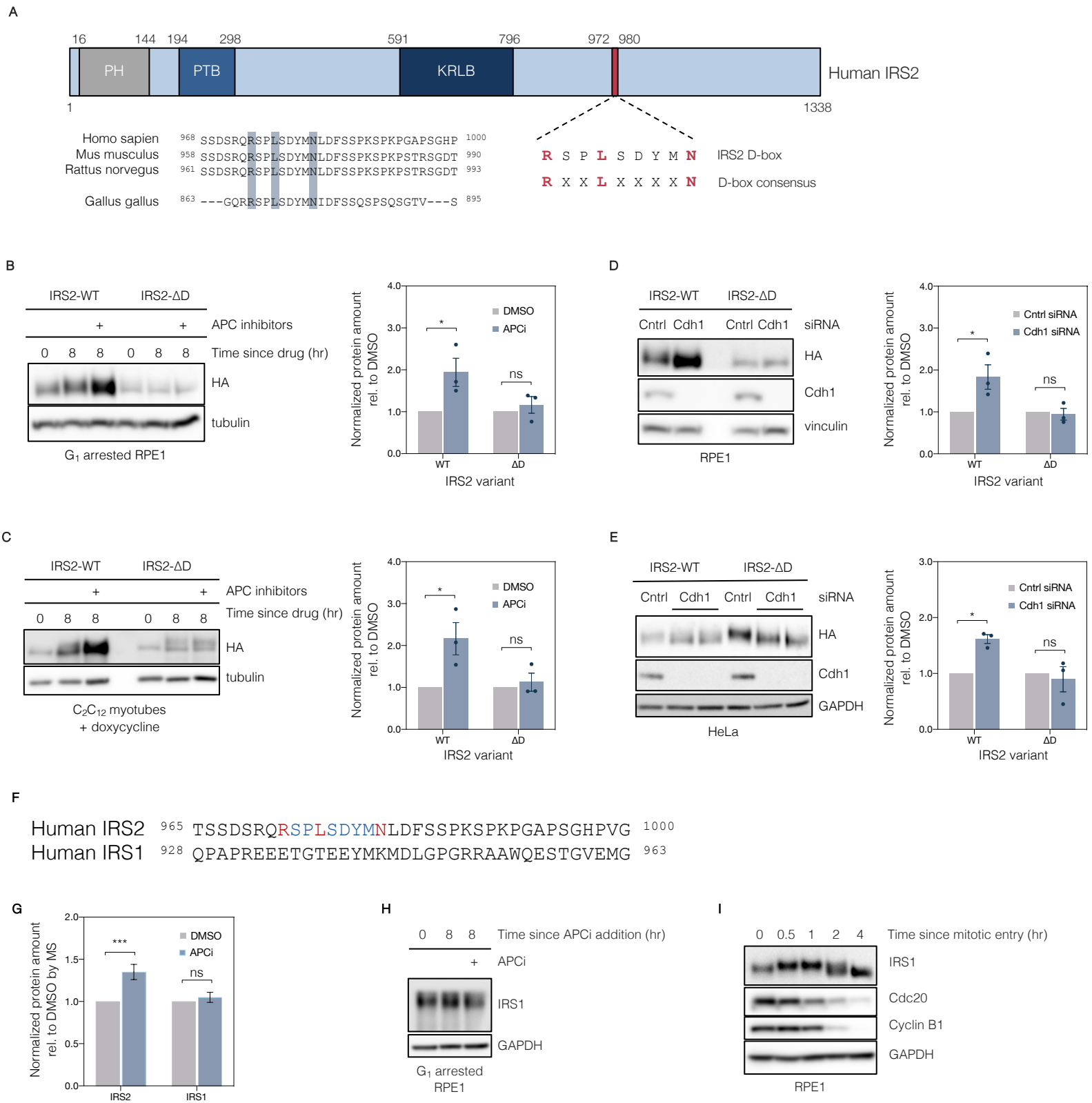
A
16
144
194
298
591
796
972
980
PH
PTB
KRLB
Human IRS2
1
1338
Homo sapien 968 SSDSRQRSPLSDYMNLDFSSPKSPKPGAPSGHP 1000
Mus musculus 958 SSDSRQRSPLSDYMNLDFSSPKSPKPSTRSGDT 990
Rattus norvegus 961 SSDSRQRSPLSDYMNLDFSSPKSPKPSTRSGDT 993
Gallus gallus 863 ---GQRRSPLSDYMNIDFSSQSPSQSGTV---S 895
R S P L S D Y M N IRS2 D-box
R X X L X X X X N D-box consensus
B
IRS2-WT
IRS2-ΔD
APC inhibitors
Time since drug (hr)
HA
tubulin
G1 arrested RPE1
Normalized protein amount rel. to DMSO
DMSO
APCi
ns
IRS2 variant
C
C2C12 myotubes + doxycycline
D
siRNA
Cntrl
Cdh1
vinculin
RPE1
Cntrl siRNA
Cdh1 siRNA
E
GAPDH
HeLa
F
Human IRS2 965 TSSDSRQRSPLSDYMNLDFSSPKSPKPGAPSGHPVG 1000
Human IRS1 928 QPAPREEETGTEEYMKMDLGPGRRAAWQESTGVEMG 963
G
Normalized protein amount rel. to DMSO by MS
IRS2
IRS1
H
Time since APCi addition (hr)
I
Time since mitotic entry (hr)
Cdc20
Cyclin B1

Figure 5

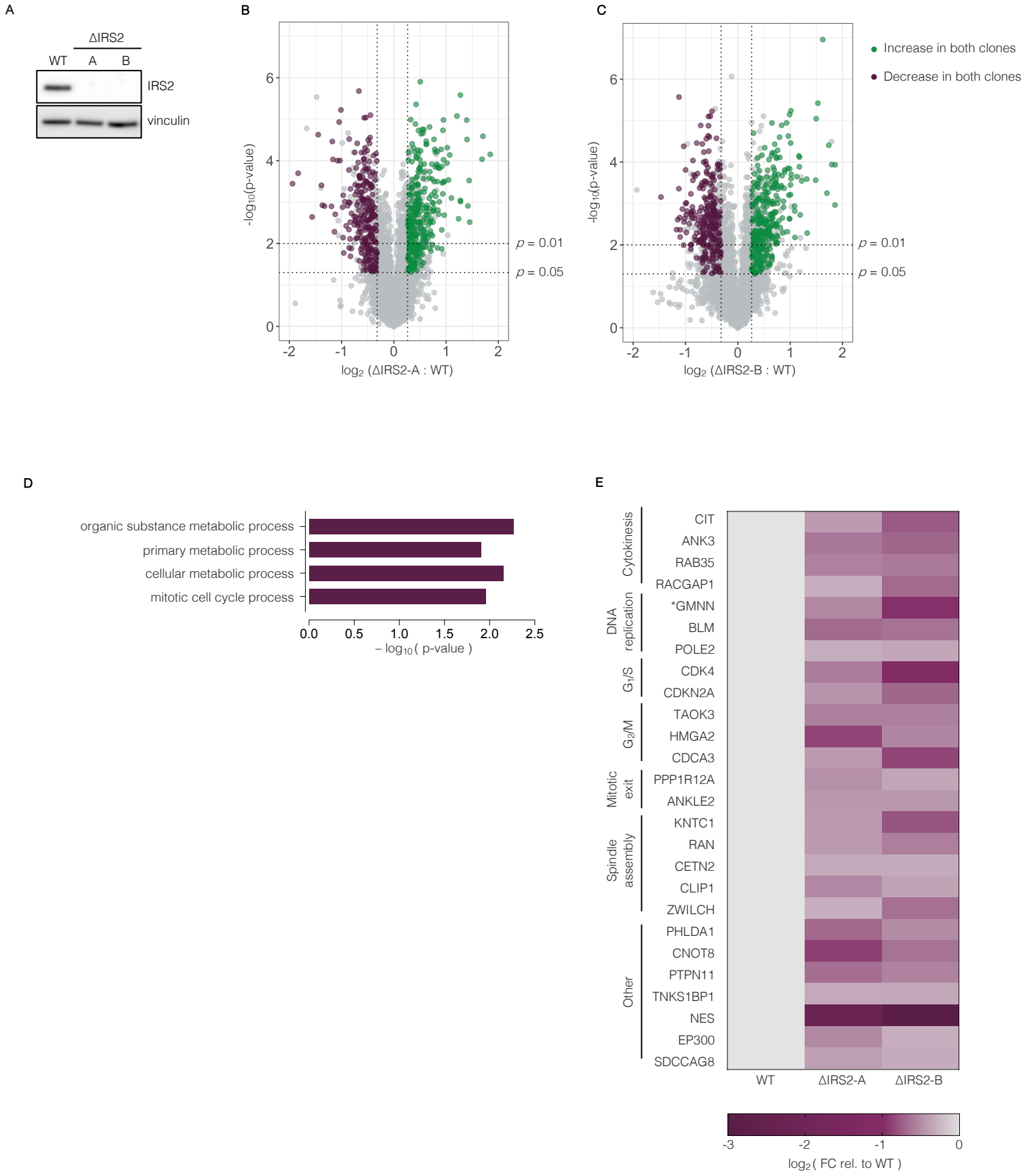
A
ΔIRS2
WT
A
B
IRS2
vinculin
B
-log10(p-value)
log2 (ΔIRS2-A : WT)
p = 0.01
p = 0.05
C
Increase in both clones
Decrease in both clones
log2 (ΔIRS2-B : WT)
D
organic substance metabolic process
primary metabolic process
cellular metabolic process
mitotic cell cycle process
– log10 (p-value)
E
Cytokinesis
DNA replication
G1/S
G2/M
Mitotic exit
Spindle assembly
Other
CIT
ANK3
RAB35
RACGAP1
*GMNN
BLM
POLE2
CDK4
CDKN2A
TAOK3
HMGA2
CDCA3
PPP1R12A
ANKLE2
KNTC1
RAN
CETN2
CLIP1
ZWILCH
PHLDA1
CNOT8
PTPN11
TNKS1BP1
NES
EP300
SDCCAG8
WT
ΔIRS2-A
ΔIRS2-B
log2 (FC rel. to WT)

Figure 6

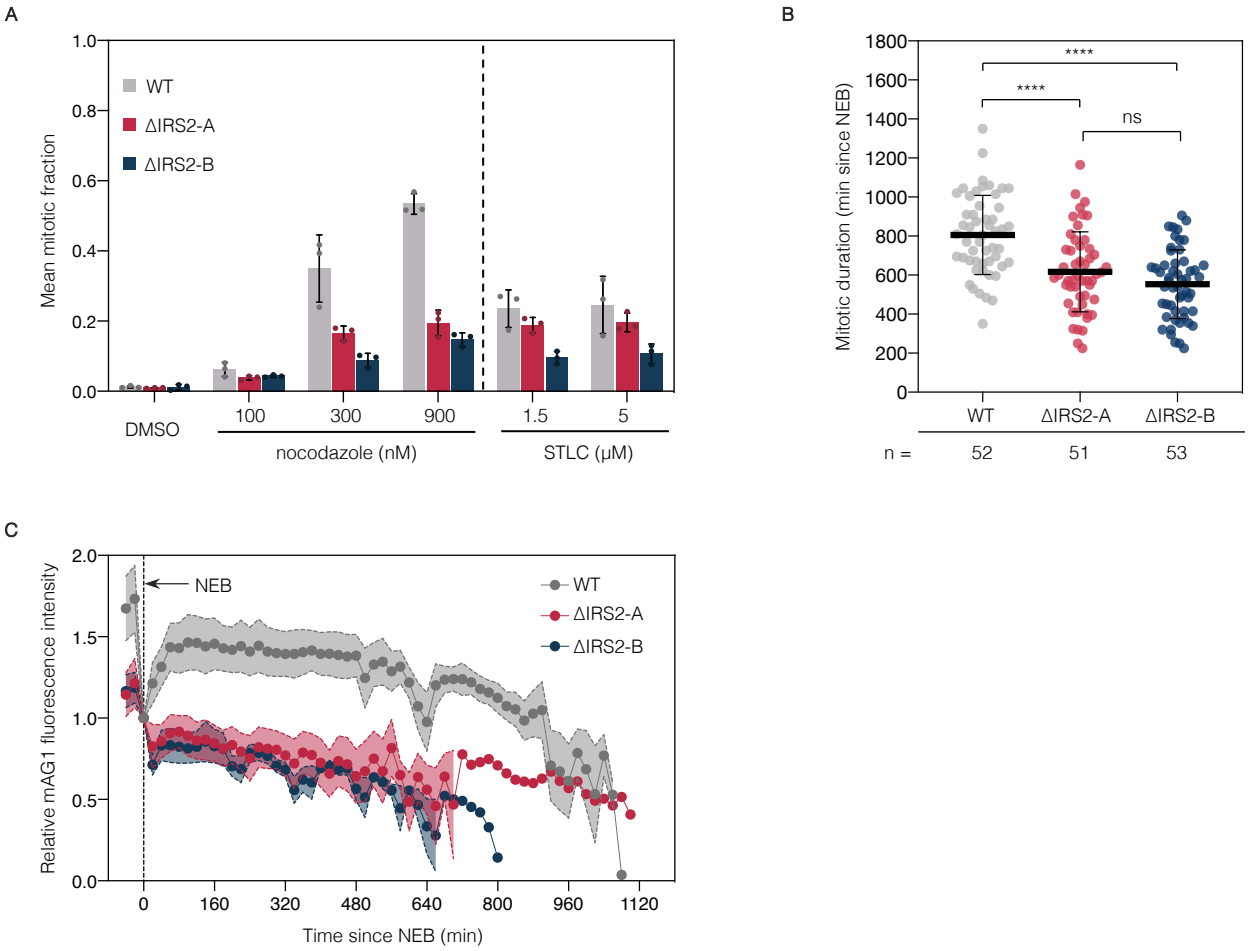
A
Mean mitotic fraction
WT
ΔIRS2-A
ΔIRS2-B
DMSO
100
300
900
1.5
5
nocodazole (nM)
STLC (μM)
B
Mitotic duration (min since NEB)
****
****
ns
WT
ΔIRS2-A
ΔIRS2-B
n =
52
51
53
C
Relative mAG1 fluorescence intensity
NEB
WT
ΔIRS2-A
ΔIRS2-B
Time since NEB (min)

Figure 7

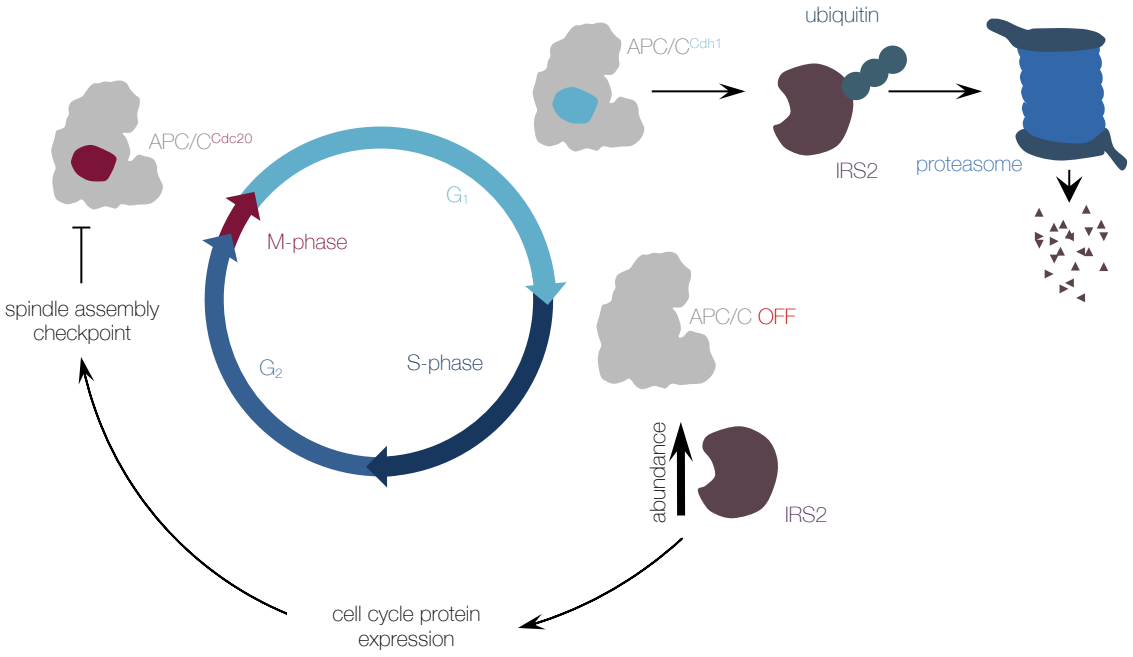
APC/C^Cdh1
ubiquitin
IRS2
proteasome
APC/C^Cdc20
G1
M-phase
spindle assembly
checkpoint
G2
S-phase
APC/C OFF
abundance
IRS2
cell cycle protein
expression